

**CLOUD TOP PROPERTIES AND CLOUD PHASE  
ALGORITHM THEORETICAL BASIS DOCUMENT**

The Schwerdtfeger Library  
University of Wisconsin-Madison  
1225 W Dayton Street  
Madison, WI 53706

W. Paul Menzel  
NOAA/NESDIS

Cooperative Institute for Meteorological Satellite Studies  
University of Wisconsin – Madison

Richard A. Frey

Cooperative Institute for Meteorological Satellite Studies  
University of Wisconsin - Madison

Bryan A. Baum

Cooperative Institute for Meteorological Satellite Studies  
University of Wisconsin – Madison

Hong Zhang

Cooperative Institute for Meteorological Satellite Studies  
University of Wisconsin - Madison

(October 2006, version 7)

## Table of Contents

1.0	Introduction	2
2.0	Overview	4
3.0	Algorithm Description	5
3.1	Theoretical Description	5
3.1.1.a	Physics of Cloud Top Properties Algorithm	5
3.1.1.b	Physical Basis of Cloud Phase Algorithm	8
3.1.2.a	Mathematical Application of Cloud Top Properties Algorithm	11
3.1.2.b	Mathematical Application of Cloud Phase Algorithm	16
3.1.3.a	Estimate of Errors of Cloud Top Properties Algorithm	17
3.1.3.b	Estimate of Errors of Cloud Phase Algorithm	27
3.2	Practical Considerations	28
3.2.1	Numerical Considerations	28
3.2.2	Programming Considerations	29
3.2.3	Validation	30
3.2.4	Quality Control	37
3.2.5	Exception Handling	38
3.2.6	Data Dependencies	38
3.2.7	Output Product	40
3.3	References	42
4.0	Assumptions	46

## 1.0 Introduction

Cloud top properties (height, temperature, and effective emissivity) are generated using the CO<sub>2</sub> slicing algorithm that corrects for possible cloud semi-transparency. The MODIS infrared CO<sub>2</sub> channels are used to investigate clouds at 5 x 5 pixel resolution (Level 2) and to generate a global cloud climatology at 1.0 degree resolution (Level 3). The MODIS bands used in our retrievals have a spatial resolution of 1 km at nadir. Additionally, an IR cloud phase is inferred from the MODIS 8.5 and 11 μm brightness temperatures at 5 x 5 pixel resolution (Level 2), and temporally averaged at 1.0 degree resolution (Level 3). This infrared technique will eventually be supplemented during daytime by the visible reflection function technique (King et al., ATBD-MOD-05) to result in a single MODIS cloud phase product. This document describes both algorithms, details the MODIS applications, and sizes the possible errors. Several references are available for further reading; for cloud top properties they are

- Baum, B. A. and B. A. Wielicki, 1994: Cirrus cloud retrieval using infrared sounding data: Multilevel cloud errors. *J. Appl. Meteor.*, 33, No. 1, 107-117.
- Baum, B. A., R. A. Frey, G. G. Mace, M. K. Harkey, and P. Yang, 2003: Nighttime multilayered cloud detection using MODIS and ARM data. *J. Appl. Meteor.*, 42, 905-919.
- Baum, B.A. and S. Platnick, 2006: Introduction to MODIS cloud products. In Earth Science Satellite Remote Sensing, Vol. 1: Science and instruments. Edited by J. J. Qu et al., Springer-Verlag.
- Chahine, M. T., 1974: Remote sounding of cloudy atmospheres. I. The single cloud layer. *J. Atmos. Sci.*, 31, 233-243.
- Eyre, J. R., and W. P. Menzel, 1989: Retrieval of cloud parameters from satellite sounder data: A simulation study. *J. Appl. Meteor.*, 28, 267-275.
- King M. D., W. P. Menzel, Y. J. Kaufman, D. Tanré, B. C. Gao, S. Platnick, S. A. Ackerman, L. A. Remer, R. Pincus, and P. A. Hubanks, 2003: Cloud, Aerosol and Water Vapor Properties from MODIS., *IEEE Trans. Geosci. Remote Sens.*, 41, pp. 442-458
- Menzel, W. P., W. L. Smith, and T. R. Stewart, 1983: Improved cloud motion wind vector and altitude assignment using VAS. *J. Clim. Appl. Meteor.*, 22, 377-384.

- Menzel, W. P. and K. I. Strabala, 1989: Preliminary report on the demonstration of the VAS CO<sub>2</sub> cloud parameters (cover, height, and amount) in support of the Automated Surface Observing System (ASOS). NOAA Tech Memo NESDIS 29.
- Menzel, W. P., D. P. Wylie, and K. I. Strabala, 1992: Seasonal and Diurnal Changes in Cirrus Clouds as seen in Four Years of Observations with VAS. *J. Appl. Meteor.*, **31**, 370-385.
- Menzel, W. P., D. P. Wylie, and K. I. Strabala, 1993: Trends in Global Cirrus Inferred from Four Years of HIRS Data. Technical Proceedings of the Seventh International TOVS Study Conference held 10-16 February in Igls, Austria.
- Naud, C. M., J. P. Muller, E. E. Clothiaux, B. A. Baum, and W. P. Menzel, 2005: Intercomparison of multiple years of MODIS, MISR, and radar cloud-top heights. *Annales Geophysicae*, Vol. **23** (7), 2415-2424.
- Platnick, S., M. D. King, S. A. Ackerman, W. Paul Menzel, B. A. Baum, and R. A. Frey, 2003: The MODIS cloud products: Algorithms and examples from Terra. *IEEE Trans. Geosci, Remote Sens.* **41**, 459-473.
- Smith, W. L., and C. M. R. Platt, 1978: Intercomparison of radiosonde, ground based laser, and satellite deduced cloud heights. *J. Appl. Meteor.*, **17**, 1796-1802.
- Wielicki, B. A., and J. A. Coakley, 1981: Cloud retrieval using infrared sounder data: Error analysis. *J. Appl. Meteor.*, **20**, 157-169.
- Wylie, D. P., and W. P. Menzel, 1989: Two years of cloud cover statistics using VAS. *J. Clim.*, **2**, 380-392.
- Wylie, D. P., W. P. Menzel, H. M. Woolf, and K. I. Strabala, 1994: Four Years of Global Cirrus Cloud Statistics Using HIRS. *J. Clim.*, **7**, 1972-1986.
- Wylie, D. P. and W. P. Menzel, 1999: Eight years of global high cloud statistics using HIRS. *Jour. Clim.*, **12**, 170-184.
- Wylie, D. P., D. L. Jackson, W. P. Menzel, and J. J. Bates, 2005: Global Cloud Cover Trends Inferred from Two decades of HIRS Observations. *Journal of Climate*, Vol. **18**, No. 15, pages 3021-3031.

For cloud phase the references are

- Ackerman, S. A., W. L. Smith and H. E. Revercomb, 1990: The 27-28 October 1986 FIRE IFO cirrus case study: spectral properties of cirrus clouds in the 8-12 micron window. *Mon. Wea. Rev.*, **118**, 2377-2388.
- Baum, B. A., P. F. Soulen, K. I. Strabala, M. D. King, S. A. Ackerman, W. P. Menzel, and P. Yang, 2000: Remote sensing of cloud properties using MODIS Airborne Simulator imagery during SUCCESS. II. Cloud thermodynamic phase. *J. Geophys. Res.*, **105**, 11,781-11,792.
- King, M. D., S. Platnick, P. Yang, G. T. Arnold, M. A. Gray, J. C. Riédi, S. A. Ackerman, and K. N. Liou, 2004: Remote sensing of liquid water and ice cloud optical thickness and effective radius in the arctic: Application of airborne multispectral MAS data. *J. Atmos. Oceanic Technol.* **21**, 857-875.
- Strabala, K. I., S. A. Ackerman and W. P. Menzel, 1994: Cloud properties inferred from 8-12 micron data. *J. Appl. Meteor.*, **33**, No. 2, 212-229.

## 2.0 Overview

Cirrus clouds are crucially important to global radiative processes and the heat balance of the Earth; they allow solar heating while reducing infrared radiation to space. Models of climate changes will have to correctly simulate these clouds to have the proper radiative terms for the Earth's heat budget. Past estimates of the variation of cloud cover and the Earth's outgoing longwave radiation have been derived primarily from the longwave infrared window (10-12 microns) radiances observed from polar orbiting and geostationary satellites (Rossow and Lacis, 1990; Gruber and Chen, 1988). The occurrence of semi-transparent clouds is often underestimated in these single channel approaches. Recently, multispectral techniques have been used to better detect cirrus in global (Wylie et al., 2005; Wu and Susskind, 1990) and North American (Wylie and Menzel, 1989) cloud studies.

Cloud phase also plays a role in regulating the Earth's energy budget; ice and water clouds react differently to similar incident radiation. For example, more absorption takes place in ice clouds between 10 and 12 microns than in water clouds of equal water content based on the indices of refraction. Therefore, changes in cloud phase will affect climate feedback mechanisms and must be included in global climate models. In the infrared window region, changes in microphysical properties from 8 to 11 microns allow these bands to differentiate cloud phase. Past infrared single band and bi-spectral split window cloud detection techniques

(Booth, 1978; Inoue, 1987; Inoue, 1989) cannot fully take advantage of these properties. There are currently two inferences of cloud phase found in the MOD06 cloud product: (1) a bispectral IR algorithm stored as a separate Science Data Set (SDS), and (2) a decision tree algorithm that includes cloud mask results as well as the IR and SWIR tests. The latter phase retrieval is stored in the MODIS "Quality\_Assurance\_1km" output SDS in addition to storage as an individual SDS in the Collection 5 processing stream. The decision tree algorithm provides the phase used in the subsequent optical and microphysical retrieval. The current IR phase algorithm is at 5-km spatial resolution, while the other two are at 1 km.

MODIS offers the opportunity to investigate seasonal and annual changes in the cirrus or semi-transparent global cloud cover and cloud phase with multispectral observations at high spatial resolution (one km rather than the current operational 17 km). Transmissive clouds that are partially transparent to terrestrial radiation can be separated from opaque clouds in the statistics of cloud cover (Wylie and Menzel, 1989). To date semi-transparent or cirrus clouds have been found in roughly 40% of all HIRS observations (Wylie et al., 1994).

### **3.0 Algorithm Description**

The theoretical basis of the algorithms and practical considerations are contained in this section.

#### **3.1 Theoretical Description**

This section discusses the physics of deriving cloud height and amount, and cloud phase from multispectral infrared radiances from a given field of view, presents the application with MODIS data, and estimates different sources of error.

##### **3.1.1.a Atmospheric Physics of Cloud Top Properties Algorithm**

MODIS cloud top pressure and effective cloud amount (i.e., cloud fraction multiplied by cloud emittance) are determined using radiances measured in spectral bands located within the broad 15-  $\mu\text{m}$  CO<sub>2</sub> absorption region. The CO<sub>2</sub> slicing technique is based on the atmosphere becoming more opaque due to CO<sub>2</sub> absorption as the wavelength increases from 13.3  $\mu\text{m}$  to 15  $\mu\text{m}$ , thereby causing radiances obtained from these spectral bands to be sensitive to a different layer in the atmosphere. The CO<sub>2</sub> slicing approach has a long history, having been applied to

data from both the High resolution Infrared Radiometer Sounder (HIRS; Wylie and Menzel 1999) and the Geostationary Operational Environmental Satellite (GOES) sounder (Menzel et al. 1992; Menzel and Purdom 1994). Error analyses for the method are provided in Menzel et al. (1992) and Baum and Wielicki (1994). The historical record of cloud properties from sounder data spans more than 25 years. MODIS provides measurements at 1-km resolution and at four wavelengths located in the broad 15  $\mu\text{m}$  CO<sub>2</sub> band. For MODIS, cloud top properties are produced for 5x5 pixel arrays wherein the radiances for the cloudy pixels are averaged to reduce radiometric noise. Thus, the CTP is produced at 5-km spatial resolution in Collection 5. It is a goal to generate CTP at both 1- and 5-km resolution in the next collection.

The MODIS cloud pressure is converted to cloud height and cloud temperature through the use of gridded meteorological products that provide temperature profiles at 25 mb intervals from 1000-900 mb, 50 mb intervals from 900-100 mb, and at 70, 50, 30, 20, and 10 mb every 6 hours. The product used for this purpose is provided by the NCEP Global Forecast System (GFS; Derber et al. 1991). Differences between model-derived and measured clear-sky radiances are mitigated with a radiance bias adjustment to avoid height assignment errors. Cloud properties are derived similarly for both daytime and nighttime data as the IR method is independent of solar illumination. CO<sub>2</sub> slicing is most effective for the analysis of midlevel to high-level clouds, especially semi-transparent clouds such as cirrus. One constraint to the use of the 15  $\mu\text{m}$  bands is that the cloud signal (change in radiance caused by the presence of cloud) becomes comparable to instrument noise for optically thin clouds and for clouds occurring in the lowest 3 km of the atmosphere. When low clouds are present, the 11  $\mu\text{m}$  data are used to infer cloud top temperature and then pressure and height via model analysis.

The CO<sub>2</sub> slicing technique is founded in the calculation of radiative transfer in an atmosphere with a single cloud layer. For a given cloud element in a field of view (FOV) the radiance observed,  $R(\nu)$ , in spectral band  $\nu$ , can be written

$$R(\nu) = (1 - NE)R_{cr}(\nu) + NE * R_{bcd}(\nu, P_c) \quad (1)$$

where  $R_{cr}(\nu)$  is the clear sky radiance,  $R_{bcd}(\nu, P_c)$  is the opaque cloud radiance from pressure level  $P_c$ ,  $N$  is the fraction of the field of view covered with cloud, and  $E$  is the cloud emissivity. It is apparent from this expression that for a given observed radiance, if the emissivity is overestimated, then the cloud top pressure is also overestimated (putting it too low in the atmosphere).

The opaque cloud radiance can be calculated

$$R_{bcd}(\nu, P_c) = R_{clr}(\nu) - \int_{P_c}^{P_s} \tau(\nu, p) \frac{dB[\nu, T(p)]}{dp} dp \quad (2)$$

where  $P_s$  is the surface pressure,  $P_c$  is the cloud pressure,  $\tau(\nu, p)$  is the fractional transmittance of radiation of frequency  $\nu$  emitted from the atmospheric pressure level ( $p$ ) arriving at the top of the atmosphere ( $p=0$ ), and  $B[\nu, T(p)]$  is the Planck radiance of frequency  $\nu$  for temperature  $T(p)$ . The second term on the right represents the decrease in radiation from clear conditions introduced by the opaque cloud.

The inference of cloud top pressure for a given cloud element is derived from radiance ratios between two spectral bands following the work of Chahine (1974) and Smith and Platt (1978). The ratio of the deviations in observed radiances,  $R(\nu)$  to their corresponding clear-sky radiances,  $R_{clr}(\nu)$  for two spectral bands of frequency  $\nu_1$  and  $\nu_2$  viewing the same FOV is written as

$$\frac{R(\nu_1) - R_{clr}(\nu_1)}{R(\nu_2) - R_{clr}(\nu_2)} = \frac{NE_1 \int_{P_c}^{P_s} \tau(\nu_1, p) \frac{dB[\nu_1, T(p)]}{dp} dp}{NE_2 \int_{P_c}^{P_s} \tau(\nu_2, p) \frac{dB[\nu_2, T(p)]}{dp} dp} \quad (3)$$

For frequencies that are spaced closely in wavenumber, the assumption is made that  $E_1$  is approximately equal to  $E_2$ , and this allows the pressure of the cloud within the FOV to be specified. The atmospheric temperature and transmittance profiles for the two spectral bands must be known or estimated.

Once a cloud height has been determined, an effective cloud amount (also referred to as effective emissivity) can be evaluated from the infrared window band data using the relation

$$NE = \frac{R(w) - R_{clr}(w)}{B[w, T(P_c)] - R_{clr}(w)} \quad (4)$$

Here  $N$  is the fractional cloud cover within the FOV,  $NE$  the effective cloud amount,  $w$  represents the window band frequency, and  $B[w, T(P_c)]$  is the opaque cloud radiance. The effective cloud amount cannot be calculated without an estimate of the window band clear sky radiance. When  $NE$  is less than unity, MODIS may be observing broken cloud ( $N < 1, E = 1$ ),



overcast transmissive cloud ( $N = 1, E < 1$ ), or broken transmissive cloud ( $N < 1, E < 1$ ). With an observational area of roughly five kilometer resolution, the semi-transparency for a given field of view is more often due to cloud emissivity being less than one than due to the cloud not completely covering the field of view; for most synoptic regimes, especially in the tropics and subtropics, this is found to be true (Wylie et al., 1994).

### 3.1.1.b Physical Basis of Cloud Phase Algorithm

The intent of the cloud phase discrimination method is to implement an infrared-only based technique that works independently of solar illumination conditions. Originally, Strabala et al. (1994) discussed the development and application of a trispectral IR technique that used bands located at 8.5, 11, and 12  $\mu\text{m}$ . This approach was simplified to a bispectral algorithm involving only the 8.5 and 11  $\mu\text{m}$  bands subsequent to the launch of the MODIS imagers. The IR phase retrieval provides four categories: *ice*, *water*, *mixed phase*, and *uncertain*. A “mixed phase” cloud is thought to consist of a mixture of ice and water particles, but is ambiguous without rigorous comparison with active depolarization data. Both the ‘mixed phase’ and ‘uncertain’ categories should be considered as undefinitive until detailed intercomparisons can be performed with the CALIPSO depolarization data.

With the bispectral IR method, cloud phase is inferred from the brightness temperature difference (BTD) between the 8.5 and 11  $\mu\text{m}$  brightness temperatures (BTD[8.5-11]) as well as the 11  $\mu\text{m}$  brightness temperature. The behavior of the IR radiances at these wavelengths for both ice and water clouds is dependent on (a) atmospheric absorption by gases such as water vapor, (b) the scattering properties of ice and water clouds, which are in turn based on particle size distributions and for ice clouds, particle habit distributions, (c) surface emissivity, and (d) cloud height.

A more complete accounting for these dependencies is provided in the references, but this section discusses the underlying physical principles that determine the capabilities and channel bandwidths of the IR cloud phase technique.

Absorption and emission by clouds are dependent upon the index of refraction of the cloud particles and their size. The index of refraction ( $m$ ) of the particle is given by

$$m = n_r - in_i, \quad (5)$$

where  $n_r$ , the real portion, is an indication of the strength of scattering by the particle, and  $n_i$ , the complex portion, is an indication of absorptive properties of the material. Figure 1 depicts the real and imaginary portions of the index of refraction at wavelengths between 8 and 13  $\mu\text{m}$  for both ice and liquid water. *Warren* (1984) provide the most recent measured data of the ice refractive index in the IR. The water refractive indices are from *Downing and Williams* (1975). The magnitude of  $n_i$  for ice and water are nearly equal between 8.5 and 10  $\mu\text{m}$  but diverge between 10 and 13  $\mu\text{m}$ . Differences in the values of the indices for water versus ice will result in distinctive reactions to similar incident radiation. If water and ice clouds were to have the same temperature (i.e., exist at the same altitude), and have similar microphysical size and shape distributions, the 8.5- $\mu\text{m}$  cloud radiance would not depend greatly on thermodynamic phase.

#### *Atmospheric Absorption in the vertical column*

MODIS radiances are influenced by atmospheric (molecular) absorption, the presence of clouds and/or aerosols and their type(s), and by surface properties. The 8.5- $\mu\text{m}$  band is sensitive to  $\text{H}_2\text{O}$ ,  $\text{O}_3$ ,  $\text{CH}_4$ , and  $\text{N}_2\text{O}$ , while the 11- $\mu\text{m}$  bands are primarily affected by  $\text{H}_2\text{O}$  and  $\text{CO}_2$ . In the RT calculations shown in Figure 2, the effects of aerosols are not included. A set of correlated- $k$  routines developed specifically for the MODIS channels are used to account for molecular absorption. These routines employ an exponential-sum fitting of transmissions (ESFT) technique (Kratz 1995; Kratz and Rose 1999) and are accurate to within 1% for clear sky conditions when compared to line-by-line calculations.

#### *Cloud Single Scattering Properties*

Cloud single scattering properties depend on the assumed size and habit distributions of the cloud particles. While water clouds are assumed to be composed entirely of spherical particles, ice clouds are generally composed of a variety of habits. The Version 1 cirrus scattering models, used in Collection 1 through Collection 4 operational processing to retrieve optical thickness and particle size, are based on mixtures of randomly-oriented hexagonal plates and columns, two-dimensional bullet rosettes, and aggregates. For Collection 5, new ice cloud bulk scattering property models (Version 2) have been implemented that are based on analyses of *in situ* microphysical cloud measurements and advances in light scattering modeling. Recent research has enabled the development of bulk scattering properties over a wider range of particle

habit and size distributions, which results in expanding and enhancing the bulk scattering model libraries used for cloud remote sensing efforts. Scattering properties are now available for a much larger set of ice particles and include droxtals, hexagonal plates, solid columns, hollow columns, aggregates, and three-dimensional bullet rosettes.

The new ice models are based on measurements from a variety of field experiments from around the world, whereas the previous set of models (Baum et al. 2000) were based on analysis of midlatitude cirrus data from the United States. An important difference between midlatitude and tropical cirrus is that the tropical cirrus formed near centers of deep convection in mesoscale systems tend to contain more particles of larger size than the synoptically-generated cirrus that forms in the midlatitudes. For most synoptically-generated midlatitude cirrus, the largest particle sizes measured are generally less than 800  $\mu\text{m}$ . Larger particles tend to settle out quickly due to the relatively low updraft velocities in the ice cloud layer. Updraft velocities tend to be much higher in mesoscale systems associated with the generation of tropical cirrus (e.g., anvils). *In situ* measurements show that, in addition to high quantities of small particles, many large particles (greater than 1 mm in diameter) are present even in the uppermost regions of tropical cirrus anvils (Heymsfield et al. 2002). The IR phase algorithm is being re-evaluated based on the use of both surface emissivity effects and the new Version 2 ice models.

#### *Cloud Height Effects: Radiative Transfer Simulations*

The RT calculations shown in Figure 2 are based on a temperature and humidity rawinsonde profile recorded on April 21, 1996 during SUCCESS (Baum et al., 2000a). This profile is very similar to a midlatitude summer regime. The low-level water cloud resides at a temperature of 284K while the cirrus is at 235K. These RT calculations indicate that the brightness temperature difference between the 8.5- and 11- $\mu\text{m}$  bands (hereafter denoted as  $\text{BTD}[8.5-11]$ ) tends to be positive in sign for ice clouds (using the Version 1 models) that have an infrared optical thickness greater than approximately 0.5. Water clouds of relatively high optical thickness tend to exhibit highly negative  $\text{BTD}[8.5-11]$  values of less than -2K. The  $\text{BTD}[8.5-11]$  values are quite sensitive to atmospheric absorption, especially by water vapor, and also to the surface emittance properties. Clear-sky  $\text{BTD}[8.5-11]$  values tend to be negative because the surface emittance at 8.5- $\mu\text{m}$  tends to be much lower than at 11  $\mu\text{m}$ , especially over non-vegetated surfaces. The  $\text{BTD}$  value for low-level water clouds tends to become more

negative as the water vapor loading increases. While a relatively small effect, multiple scattering is included in radiative transfer simulations of the BTD[8.5-11]. Small particles tend to increase the BTD[8.5-11] values relative to large particles because of increased scattering.

### *IR Cloud Phase Determination*

Given these caveats, the simple bispectral IR technique shown in Figure 3 is adequate for classifying the phase as either “ice” or “water” for about 80% of the cloudy pixels on a global basis, regardless of solar illumination. The most problematic areas are optically thin cirrus, multilayered clouds (especially thin cirrus over lower-level water clouds), and single-layered clouds having cloud top temperatures between 233K and 273K (i.e., supercooled water or “mixed phase” clouds). Supercooled water or mixed-phase clouds tend to occur most frequently in the high latitude storm belts of both hemispheres. When ice and water clouds are well separated in height, the BTD[8.5-11] values, in conjunction with the 11- $\mu\text{m}$  BT, are adequate for phase discrimination. The use of CALIPSO depolarization data will be instrumental in understanding the radiative signature from the IR bands.

#### 3.1.2.a Mathematical Application of Cloud Top Properties Algorithm

The MODIS radiometer senses infrared radiation in seventeen spectral bands that lie between 3.75 and 14.24  $\mu\text{m}$  at 1 km resolution (depending upon viewing angle) in addition to visible reflections at the same or better resolution. The four channels in the  $\text{CO}_2$  absorption band (ch 33 at 13.34, ch 34 at 13.64, ch 35 at 13.94, and ch 36 at 14.24  $\mu\text{m}$ ) are used to differentiate cloud altitudes and the longwave infrared window channel (ch 31 at 11.03  $\mu\text{m}$ ) identifies the effective emissivity of the cloud in the MODIS field of view (FOV). Figure 4 indicates the weighting functions for the  $\text{CO}_2$  absorption channels on MODIS.

Equation (3) will nominally be used to determine the mean cloud properties from a 5 x 5 FOV. On the left side of Equation (3), cloud radiances are determined by averaging only the radiances for those FOVs designated to be probably cloudy or cloudy by the cloud mask (at least 4 must be flagged); this enables signal to noise ratio enhancement. Clear radiances are calculated in a radiative transfer calculation of the MODIS spectral band radiances using a transmittance model called Pressure layer Fast Algorithm for Atmospheric Transmittances (PFAAST) (Hannon et al. 1996); this model has 101 pressure level vertical coordinates from

0.05 to 1100 hPa. The calculations take into account the satellite zenith angle, absorption by well-mixed gases (including nitrogen, oxygen, and carbon dioxide), water vapor (including the water vapor continuum), and ozone. The global analyses of temperature and moisture fields from the National Center of Environmental Prediction (NCEP) and Reynolds blended sea surface temperatures (Reynolds and Smith, 1994) are used to define the fields of temperature and moisture used in the forward calculation.

The right side of Equation (3) is calculated from a temperature and moisture profile and the profiles of atmospheric transmittance for the spectral bands as a function of  $P_c$ , the cloud top pressure (the integration through the atmosphere is accomplished at discrete intervals and the best pressure level interpolated to the nearest 5 mb). Again, the NCEP global analyses of temperature and moisture fields are used. A radiance bias adjustment of measured versus calculated clear sky radiances is incorporated based on the previous eight day clear sky radiance composite; this adjustment is necessary to assure that the right and left sides of Equation (3) are balanced.

With the assumption that the emissivity of the clouds is the same for the two spectral bands, the  $P_c$  that best matches measured and calculated ratios is deemed a candidate solution for the cloud top pressure; the search is restricted between the surface pressure (or the top of the inversion layer) and the tropopause.

The cloud top pressure is selected with a “top-down” approach. If the most opaque bands (e.g. 14.24  $\mu\text{m}$  /13.94  $\mu\text{m}$ ) detect cloud so that  $(R - R_{clr})$  for both bands is greater than the instrument noise (conservatively estimated at roughly 1  $\text{mW}/\text{m}^2/\text{ster}/\text{cm}^{-1}$ ) and Equation (3) produces a solution high in the troposphere, this is taken as the cloud top pressure solution (no other band ratios are investigated). This ratio is most sensitive to the highest clouds. If the most opaque bands do not produce a solution, a ratio of less opaque bands (e.g. 13.94  $\mu\text{m}$  /13.64  $\mu\text{m}$ ) is investigated for a solution in the upper part of the troposphere; if found this is taken as the cloud top pressure solution (no other bands are investigated). This ratio is generally more sensitive to middle-level clouds and cloud edges where information from the atmosphere below is important. If the less opaque bands do not produce a solution, a ratio of even less opaque bands (e.g. 13.64  $\mu\text{m}$  /13.34  $\mu\text{m}$ ) is investigated. This would yield the cloud top pressure for the lowest level clouds.

Thus for Aqua MODIS, ratios 36/35, 35/34, and 34/33 are used (14.24  $\mu\text{m}$  / 13.94  $\mu\text{m}$ , 13.94  $\mu\text{m}$  / 13.64  $\mu\text{m}$ , and 13.64  $\mu\text{m}$  / 13.34  $\mu\text{m}$ , respectively). Since Terra MODIS has severe noise problems in band 34, only ratios 36/35 and 35/33 are used.

If  $N_c$  is the number of cloudy pixels within the 5 x 5 array (estimated using the cloud mask of Ackerman et al., ATBD-MOD-06), then the representative effective cloud amount for the 5 kilometer area will be the NE determined for the cloudy pixels adjusted to represent all the pixels in the 5 x 5 array (e.g.  $NE_{5x5} = N_c * NE / 25$ ). The cloud top temperature is taken as the brightness temperature indicated by the GFS temperature profile for level of the cloud top pressure (Menzel and Gumley, ATBD-MOD07).

If a radiance ratio cannot be calculated reliably for any of the possible band pairs because  $(R - R_{clr})$  is within the instrument noise level, then a cloud top pressure is calculated directly from the infrared window band (assuming it has adequate signal to noise). The MODIS observed 11.03  $\mu\text{m}$  infrared window band brightness temperature is compared with a corresponding brightness temperature profile derived from the gridded model product to infer a cloud top pressure and the cloud emissivity is assumed to be unity and  $NE=N_c/25$ . In this way, all clouds are assigned a cloud top pressure either by  $\text{CO}_2$  or infrared window calculations. Very thin high cloud are sometimes mistaken for low level opaque clouds; Wylie and Menzel (1989) found that this occurred for about half of the very thin clouds with NE less than 10%.

In summary, the calibrated and navigated MODIS data are processed for 5x5 pixel areas. Fields of view are determined to be clear or cloudy from the cloud mask (Ackerman et al. ATBD-MOD35). In the case where all 22 to 25 of the 1 km FOV's are clear, no cloud parameters are calculated. The data also will be corrected for zenith angle to minimize the impact of the increased path length through the atmosphere of radiation upwelling to the satellite. Global coverage is realized every two days with one satellite.

(1) In Equation (3), the LHS (left hand side) is determined using the average of the measured cloudy radiances in the 5 x 5 pixel area minus a forward calculated clear radiance for the  $\text{CO}_2$  slicing bands. The NCEP global model is used to calculate the clear radiances; these forward calculated radiances must still be adjusted for radiance bias (calculated - measured clear radiance) inferred for clear FOVs from the previous eight days. The same global model is used to calculate the RHS (right hand side) for a distribution of cloud top pressures; this calculation is performed only at the grid spacing of the model.

(2)  $P_c$  derived from the most opaque bands and the associated window band NE is calculated for the cloudy subset of pixels.

(3) NE for the 5 x 5 array is then determined from  $NE_{5 \times 5} = N_c * NE / 25$

(4) If cloud forcing is too small (within instrument noise), an infrared window band solution, assuming a low opaque cloud, is used for the cloudy pixels and  $NE_{5 \times 5} = N_c / 25$ .

The accuracy of the cloud retrieval depends on good calibration, knowledge of spectral response functions, and accurate and computationally fast radiative transfer models to simulate top-of-atmosphere radiances. For the Aqua MODIS imager, the knowledge of spectral response functions (SRF) for the 13.9  $\mu\text{m}$  and 14.2  $\mu\text{m}$  bands has been improved through comparison with AIRS spectra. The difference between calculated and observed clear-sky radiances for the CO<sub>2</sub> slicing spectral bands is mitigated with a radiance bias adjustment. Finally, cloud top properties also depend on the sensor view angle. These considerations are discussed below.

As reported in Tobin et al. (2005), comparisons of co-located AIRS and MODIS observations show radiance differences in MODIS bands 33 through 36 that have significant dependency on scene temperature. They show that AIRS and MODIS radiance differences for the same scene are much smaller when the MODIS spectral response function (SRF) is shifted slightly. The temperature dependence is also greatly reduced. While the AIRS-MODIS radiance comparisons are improved through a slight shift in the SRF, no cause has been identified why such a shift could occur.

Moreover, it is important to note that these SRF adjustments do not correct for observed minus calculated radiance differences. Inspection of global fields of observed minus calculated clear sky radiances using the shifted SRFs do not show a global improvement. A latitudinal structure in the biases remains evident; shifting the SRF reduces polar and mid-latitude biases but increases equatorial biases. A latitudinal radiance bias adjustment (possibly indicating temperature dependence in the bias) is needed to mitigate these differences.

Measured and calculated clear sky radiances differ because of the cumulative effects of instrument noise, spectral response function errors, inadequate knowledge of the atmospheric and surface state, and radiative model approximations. An adjustment is necessary to balance the right and left sides of Equation (3).

A clear sky 1° latitudinally averaged bias adjustment is created from the 8-day clear sky bias file. The biases are composited and stored separately by day, night, land and water for the

MODIS CO<sub>2</sub> absorption bands (bands 33-36). For example biases from 23-30 November 2004, used in processing 1 December 2004, range from -0.2 to +0.5 mW/m<sup>2</sup>/ster/μm over land and from -0.1 to +0.2 mW/m<sup>2</sup>/ster/μm over oceans. Note that land values are used for ocean ice cases in the Antarctic region. The pre-computed zonal biases are added to calculated clear-sky radiances needed for each CO<sub>2</sub> slicing CTP retrieval. Figure 5 shows the CTPs before and after application of the bias corrections for two 1 December 2004 granules. Note that more of the transmissive cirrus is now being reported as high cloud. Cloud heights are impacted more in the middle and high latitudes and less in the deep tropics. On this day, the amount of retrieved high-level transmissive clouds increased by 10% and 13% in the northern and southern mid-latitudes, respectively. There was an increase of 11% and 21% additional CO<sub>2</sub>-slicing retrievals (as opposed to those from the 11 μm window) in these same regions. The radiance biases were tested globally on mid-winter, mid-summer, and transition season data; in all cases the results were more in family with other observations from lidar backscatter and HIRS CO<sub>2</sub> slicing.

The effect of the radiance bias adjustment is further illustrated in Figure 6 where MODIS cloud top heights are compared with backscatter data from the Cloud Physics Lidar (McGill et al., 2002) data. The radiance bias adjustment was not implemented until Collect 5; Collect 4 is largely the same algorithm except for the radiance bias considerations. Figure 6 shows that the radiance bias adjustment moves the cloud top heights (cloud top pressures converted to heights using a pressure versus geopotential height profile) from Collect 4 up about 3 km; this places Collect 5 heights within the cloud extent determined from the CPL whereas in Collect 4 they were well below the cloud bottom.

The “top-down” approach is different from earlier CO<sub>2</sub> slicing approaches. As described in Menzel et al. (1983), cloud top pressures were previously determined from the various ratios (14.24 μm /13.94 μm, 13.94 μm /13.64 μm, 13.94 μm /13.34 μm, 13.64 μm /13.34 μm) and the most representative cloud height and amount are those that best satisfy the radiative transfer equation for the four CO<sub>2</sub> bands and the infrared window. An example granule using the “top down” approach is shown in Figure 7 along with the “CO<sub>2</sub> radiative minimum” approach (where valid cloud pressures and corresponding effective cloud amounts are used in an error minimization technique based on radiative transfer calculations). The top down algorithm shows fewer (presumably) spurious high clouds.



### 3.1.2.b Mathematical Application of the Cloud Phase Algorithm

While the original MODIS IR phase approach was based on the use of the 8.5, 11, and 12- $\mu\text{m}$  bands, the results obtained from operational testing uncovered some problems. The essence of the tri-spectral method consisted of interpreting a scatter diagram of BTD[8.5-11] versus BTD[11-12] values. To obtain a scatter plot of such values, an entire MODIS scan line was processed at one time. Much of the testing prior to the launch of MODIS involved the use of MODIS Airborne Simulator (MAS) data, or with case studies using the lower spatial resolution HIRS-10 instrument, which was the only satellite that contained all three IR bands. The MAS data was collected primarily in the midlatitude region in the Northern Hemisphere and did not tend to include midlevel, mixed phase clouds. When working with MAS data, at 50-m pixel resolution, certain problems were never encountered such as scenes that contain clouds at multiple levels. When applied to MODIS scan lines, with a much greater swath width, data from low clouds over water in one part of the scan were mixed with data from high clouds over land in another part of the same scan line.

Another problem encountered during initial operational application of the trispectral algorithm was that the slopes between the BTD[8.5-11] and BTD[11-12] values were often close to zero, thereby confusing the algorithm. This problem was noted for clouds at temperatures between approximately 250K and 270K. One topic that hadn't been adequately addressed during the testing phase was the ability to discriminate between ice and water particles at cloud top when the clouds may contain primarily supercooled water droplets or perhaps a mixture of both ice and water (i.e., mixed phase). Single-layered clouds of wide spatial extent having cloud-top temperatures in the range between 250K and 270K are prevalent in the storm tracks in both the Northern and Southern Hemispheres. These clouds are extremely difficult to discriminate phase for unambiguously. Current efforts are to improve cloud phase discrimination for clouds at temperatures between 233K and 273K, the range over which the presence of supercooled water is possible.

Furthermore, optically thin cirrus is very difficult to detect, the estimation of phase is often ambiguous. To ameliorate these and other problems, the approach was distilled and simplified so that it could be applied to any individual pixel or averaged group of radiances. Currently, cloud phase is inferred from analysis of the 8.5- and 11- $\mu\text{m}$  brightness temperatures.

The MODIS 8.5- and 11- $\mu\text{m}$  bands are used to determine cloud phase over a 5 pixel x 5 pixel area. The MODIS cloud mask (MOD35) provides a pixel-level product that identifies pixels which are unobstructed (i.e., clear sky). The brightness temperatures for each band for a given FOV are averaged over each 5 by 5 pixel box. As the implementation now being used does not rely on analyses of scatter plots, as did the original code, the method may easily be applied to each pixel if desired.

### 3.1.3.a Estimate of Errors of Cloud Top Properties Algorithm

In the study of Wylie and Menzel (1989), the  $\text{CO}_2$  cloud heights derived from VAS (VISSR Atmospheric Sounder) data over North America were found to be of good quality when compared to three other independent sources of cloud height information. Results showed: (a) for about thirty different clouds, the  $\text{CO}_2$  heights were within 40 mb rms of cloud heights inferred from radiosonde moisture profiles; (b) in 100 comparisons with lidar scans of clouds, the  $\text{CO}_2$  heights were 70 mb lower on the average and were within 80 mb rms; (c) satellite stereo parallax measurements in 100 clouds compared to within 40 mb rms. The  $\text{CO}_2$  heights appeared to be consistent with other measurements within 50 mb and the effective fractional cloud cover within 0.20 in most cloud types. The  $\text{CO}_2$  slicing technique works best for middle and high clouds, but has trouble with very low clouds.

#### 3.1.3.a.1 Errors Associated with the Assumption of Constant Emissivity

Spectrally close channels are used to minimize differences in the cloud emissivity between the two spectral channels. Calculations by Jacobowitz (1970) indicate that negligible error occurs in the cloud top pressure estimation using the assumption of constant emissivity for the  $\text{CO}_2$  channels between 13.3 and 14.2 microns.

#### 3.1.3.a.2 Errors Associated with the Assumption of a Thin Cloud Layer

The  $\text{CO}_2$  slicing algorithm assumes that all of the radiative effects of the cloud occur in the top thin layer. This makes the mathematics tractable. If the radiative transfer integral of Equation (3) were to include a cloud term where the cloud has finite depth, then a knowledge of the vertical structure of the cloud would be required. There are an infinite variety of combinations of cloud depths and vertical combinations that could produce the same integrated

radiative signature; a unique solution is not possible. Any initial assumption of cloud structure biases the cloud top and bottom solution derived in the radiative transfer formulation.

The thin layer cloud approximation is investigated in Smith and Platt (1978). They found that errors in the height assignment approaching one-half (one-quarter) the thickness of the cloud were introduced for optically thin (thick) clouds where the integrated emissivity is less than (greater than) .6. The largest errors will be associated with physically thick but optically thin cirrus clouds. For optically thin (very transparent) cirrus with 100 mb depth the error in the height estimate is roughly 50 mb.

Wielicki and Coakley (1981) also discussed the consequences of the thin layer cloud approximation. They concluded that the algorithm solution ( $P_c$ ) would be near the center of the cloud for optically thin clouds and near the top of the cloud for optically thick clouds. This is similar to a center of mass concept. The algorithm solution will thus be close to the "radiative center" of the cloud. Thus,  $P_c$  is somewhere between the cloud top and its center varying with the density of the cloud.

Cirrus height errors are also discussed in Wylie and Menzel (1989) where VAS cloud top pressure estimates were compared to cloud tops measured by lidars and by the stereo parallax observed from the images of two satellites at two different viewing angles. VAS CO<sub>2</sub> channels (14.25, 14.01, and 13.33 microns) are similar to three of the four on MODIS. In the lidar comparison, the VAS inferred cloud top pressure over an observation area was compared to the highest lidar observation in the same area; these clouds had to be radiatively thin for the lidars to see through to the tops. Definition of a single cloud top was often difficult within a cloud layer; the lidar heights varied considerably (by more than 50 mb) from one cloud element to another in the same cloud layer. On the average, the VAS  $P_c$  was found to be 70 mb larger (lower cloud altitude) than the tops seen on the lidars. The CO<sub>2</sub> slicing technique was sensing the mean height; the VAS heights were comparable to the lidar top heights to within half the cloud thickness. In the comparisons to stereo parallax measurements for thin transmissive clouds, the VAS heights showed little bias. It was often difficult to measure parallax for thin transmissive clouds, as they appeared fuzzy with poorly defined boundaries in the images. Since the image of the clouds is more indicative of the center of the diffuse cloud mass than its outer boundaries, the parallax method is also sensitive to the radiative center of mass rather than the physical tops of

these clouds. Thus, in these intercomparisons of actual measurements, the CO<sub>2</sub> cloud top pressures were found to be within the accuracy suggested by theoretical considerations.

### 3.1.3.a.3 Errors Associated with the Presence of a Lower Cloud Layer

The algorithm assumes that there is only one cloud layer. However, for over 50% of satellite reports of upper tropospheric opaque cloud, the ground observer indicates additional cloud layers below (Menzel and Strabala, 1989). To understand the effects of lower cloud layers, consider the radiation sensed in a cloudy field of view. For a semi-transparent or cirrus cloud layer, the radiation reaching the satellite,  $R$ , is given by

$$R = R_a + E * R_c + (1 - E) * R_b \quad (10)$$

where  $R_a$  is the radiation coming from above the cloud,  $R_c$  is the radiation coming from the cloud itself,  $R_b$  is the radiation coming from below the cloud, and  $E$  is the cloud emissivity. When a lower cloud layer is present under the semi-transparent or cirrus cloud,  $R_b$  is smaller (i.e., some of the warmer surface is obscured by the colder cloud). If prime indicates a two layer cloud situation of high semi-transparent cloud over lower cloud, and no prime indicates a single layer high semi-transparent cloud, then

$$R_b' < R_b, \quad (11)$$

which implies

$$R' < R. \quad (12)$$

Thus the difference of cloud and clear radiance is greater for the two layer situation,

$$[R_{clr} - R'] > [R_{clr} - R] \quad (13)$$

The effect of two cloud layers is greater for the 13.3 micron channel than for the other CO<sub>2</sub> micron channels, because the 13.3 micron channel "sees" lower into the atmosphere (Figure 4 shows the weighting functions where the 13.3 peaks lower in the atmosphere than the other CO<sub>2</sub> channels). So using the 13.9/13.3 ratio as an example

$$[R_{clr}(13.3) - R'(13.3)] > [R_{clr}(13.9) - R'(13.9)] \quad (14)$$

This reduces the ratio of the clear minus cloud radiance deviation in Equation (3) because the denominator is affected more than the numerator (when the less transmissive channel is in the numerator),

$$\frac{[R_{clr}(13.9) - R'(13.9)]}{[R_{clr}(13.3) - R'(13.3)]} < \frac{[R_{clr}(13.9) - R(13.9)]}{[R_{clr}(13.3) - R(13.3)]}, \quad (15)$$

or  $Left' < Left$ , where  $Left$  refers to the left side of Equation (3). An example plot of  $P_c$  versus  $Right$  (where  $Right$  refers to the right side of Equation (3)), shown in Figure 8, indicates that  $Left' < Left$  implies  $P_c' > P_c$ . Thus, when calculating a cloud pressure for the upper semi-transparent cloud layer in a two cloud layer situation, the CO<sub>2</sub> slicing algorithm places the upper cloud layer too low in the atmosphere.

An example from 25 October 1990 using VISSR Atmospheric Sounder (VAS) data is presented to illustrate further the magnitude of the errors that can be induced by lower level clouds (results for other days and other situations were found to be comparable). Ground observers in Omaha, Nebraska reported thin cirrus clouds with no other underlying clouds present. The ratio of the 13.9 to 13.3 micron satellite observed radiance differences between clear and cloudy FOVs (the left side of Equation (3)) is 0.36 on 25 October. This implies single layer cloud at 300 mb (solving the right side of Equation (3) for  $P_c$  as shown in Figure 8).

$R'$  has been modeled for a semi-transparent cloud at 300 mb with an underlying opaque cloud layer at 920, 780, 670, 500, and 400 mb (each configuration produces a different ratio in the left side of Equation (3),  $Left'$ ). The different  $Left'$  suggest different  $P_c'$  solutions as  $Left'$  is matched to  $Right$ , the right side of Equation (3). In the absence of any knowledge of a lower layer, the CO<sub>2</sub> algorithm integrates the right side of Equation (3) from the surface to an incorrect  $P_c'$ . Figure 8 shows  $Right$  as a function of  $P_c$  for the situation of 25 October. The errors in calculated cloud top pressure from the original 300 mb solution,  $P_c' - P_c$ , are shown as a function of height of the underlying opaque cloud layer in Figure 9a for 25 October.

In the two cloud layer situation, the position of the lower cloud layer affects the accuracy of the estimate of the height of the upper cloud layer. Opaque clouds in the lower troposphere underneath high cirrus have little affect on the cirrus  $P_c$ . Inspection of the spectral transmittance show that neither the 14.2 or the 13.9 micron channels are very sensitive to radiation from low in the troposphere, while the 13.3 micron channel senses only about half of the radiation from below 800 mb. Opaque clouds in the middle troposphere, between 400 and 800 mb, underneath high cirrus, cause the cirrus  $P_c$  to be overestimated (lower in the atmosphere) by up to 220 mb

(this extreme occurs for the very thin high cirrus cloud with NE of 0.10). The decreases in  $R_b$  produce smaller ratios for the left side of Equation (3) which in turn produces larger estimates of  $P_c$ . Opaque clouds high in the atmosphere, underneath higher cirrus, have little effect on the cirrus  $P_c$ , since the height of the lower opaque layer approaches the height of the semi-transparent upper cloud layer and the CO<sub>2</sub> algorithm is going to estimate a height in between the two layers.

The errors in  $P_c$  were also examined for different emissivities of transmissive clouds (see Figure 9b). This was modeled by varying the emissivity and forming new ratios on the left side of Equation (3). The maximum cloud top pressure error of roughly 220 mb occurred in very thin cloud with emissivity of 0.10. The error in  $P_c$  reduced as the emissivity of the transmissive clouds increased. For a cloud with emissivity of 0.5, the maximum error in  $P_c$  is about 100 mb. For more dense clouds with emissivity of 0.9, the maximum error in  $P_c$  is less than 20 mb. The VAS data have shown a nearly uniform population of emissivity center around 0.5 (Wylie and Menzel, 1989), so one can conclude that the errors in the cloud top pressure caused by underlying clouds should average under 100 mb.

Multi-layer cloud situations (transmissive over opaque cloud) cause the height estimate of the upper cloud to be about 100 mb too low in the atmosphere on the average. The error in transmissive cloud height is largest when the underlying opaque layer is in the middle troposphere (400- 700 mb) and small to negligible when the opaque layer is near the surface or close to the transmissive layer. The error in effective emissivity increases as the opaque layer approaches the transmissive layer; when they are coincident, the effective emissivity is assumed to be one. In summary the cloud forcing from two layers is greater than the cloud forcing from one layer; assuming only one cloud layer when two exist causes the CO<sub>2</sub> solution to put the cloud between the two layers with larger effective emissivity. This suggests that, overall, global cloud parameter estimates will be a little low in the atmosphere and with an effective emissivity a little too high.

Recent work has suggested that the radiative transfer equation in a two layer cloud situation can be solved from the CO<sub>2</sub> radiance observations. The two layer cloud forcing can be written, where  $u$  is the upper cloud layer and  $l$  is the lower cloud layer,

$$R - R_{clr} = N_l E_l \left[ 1 - N_u E_u \right] \int_{P_s}^{P_{cl}} \tau dB + N_u E_u \int_{P_s}^{P_{cu}} \tau dB \quad (16)$$

Thus the two layer cloud forcing is characterized by four unknowns  $N_l E_l$ ,  $N_u E_u$ ,  $P_{cl}$ , and  $P_{cu}$ . Using the measured cloud forcing in the CO<sub>2</sub> channels, a solution for upper and lower cloud pressures and effective cloud amounts is calculated. The algorithm selects spectrally close pairs of CO<sub>2</sub> channels. For each pair of cloud forcing measurements, all possible  $N_l E_l$ ,  $N_u E_u$  are calculated as a function of  $P_{cl}$ ,  $P_{cu}$ . From this array of possible solutions, the selected solution best satisfies the radiative transfer equation for all spectral channels. Since four unknowns offer more degrees of freedom than two unknowns, the two layer solution is preferred over the one layer solution. Indication of when to use the two layer solution is sought through inspection of 4.0 micron versus 11.0 micron radiance scatter plots for the 5 x 5 pixel area (when radiances for the two spectral channels lie on two or more straight lines then the presence of two or more cloud layers is suggested). More development work remains, before the two layer solution can be incorporated into the cloud parameter algorithm.

#### 3.1.3.a.4 Errors from an Inaccurate Estimate of the Surface Temperature

The CO<sub>2</sub> slicing algorithm has little sensitivity to surface temperature. The weighting functions for the CO<sub>2</sub> channels indicate that very little radiation from the Earth surface is detected by the satellite radiometer in these spectral bands (14.2 and 13.9 micron observations don't even see the ground). Table 3 indicates the changes in cloud top pressure associated with changes in estimates of surface temperature inferred from a recalculation of the right side of Equation (3); the atmospheric profile of 25 October was used as an example (other situations yield similar results). When the surface temperature  $T_{sfc}$  is assumed to be 5 C too warm, the cloud top pressure  $P_c$  is 32 mb smaller (higher in the atmosphere); when  $T_{sfc}$  is assumed to be 5 C too cold,  $P_c$  is 26 mb larger (lower in the atmosphere). In other words, when the surface temperature guess doesn't track surface warming (cooling), then the cloud layer is calculated to be too low (high).

Table 3 also indicates an additional effect that arises when the surface temperature is assumed to be too cold. In the cloud screening process, some cloudy FOVs are inferred to be clear and  $R_{clr}$  is reduced for all spectral channels. Thus the left side of Equation (3) is reduced

(when the less transmissive channel is in the numerator) and  $P_c$  goes even larger (lower in the atmosphere). The last four columns of Table 3 show the total error when 25% of the FOVs are incorrectly inferred to be clear for a guess that is 5 C too cold; when high clouds at 300 mb contaminate the clear radiance determination,  $P_c$  is 39 mb larger (representing an additional error of 13 mb), and when low clouds at 700 mb contaminate the clear radiance determination,  $P_c$  is 20 mb larger (representing an offsetting error of 6 mb).

**Table 3. The changes in cloud top pressures ( $P_c$ ) and effective emissivities determined from the CO<sub>2</sub> slicing algorithm after changes to the estimated temperature profile and surface temperature (using the data of 25 October 1990).**

Guess Error (guess - truth)			Cloud Top Pressure and Effective Emissivity Error							
							with additional errors from faulty cloud screening for contaminating clouds at			
met	sfc	atm			300mb		700mb			
cond	$DT_s$	$DT_{(p)}$	$DP_c$	$D(NE)$	$DP_c$	$D(NE)$	$DP_c$	$D(NE)$		
a	+5 K	0 K	-32 mb	-.09						
b	-5	0	+26	+.13	+39 mb	+.13	+20 mb	+.09		
d	0	+2	+10	+.03						
c	0	-2	-13	-.03						
ad	+5	+2	-20	-.07						
ac	+5	-2	-44	-.11						
bd	-5	+2	+37	+.19	+50	+.19	+31	+.14		
bc	-5	2	+16	+.09	+28	+.09	+09	+.06		

Possible meteorological conditions that could cause indicated errors in the guess

- a indicates nocturnal cooling
- b indicates solar heating
- c indicates warm frontal passage
- d indicates cold frontal passage

The surface temperatures are monitored hourly with the SVCA conventional observations; errors of 5 C are unusual, but do occur in the western mountains where surface observations are too sparse to accurately represent the varying altitude conditions. We conclude that nominal diurnal changes in surface temperature will not affect the CO<sub>2</sub> slicing solutions of  $P_c$  by more than 50 mb.



Furthermore, fictitious reports of transmissive clouds cannot be produced by changes in the ground surface temperature, since two of the three channels do not see the ground. As witnessed in Table 3, effective emissivity estimates are relatively insensitive to surface temperature excursions of 5 C; NE changes of about 0.10 are found.

The preceding discussion also implies that the CO<sub>2</sub> algorithm is insensitive to surface emissivity changes since 5% changes in surface temperature can be equated with roughly 7% changes in surface emissivity for the long wavelength channels.

#### 3.1.3.a.5 Errors from an Inaccurate Estimate of the Temperature Profile

Table 3 also shows the changes in cloud top pressure associated with changes in estimates of temperature profile as well as surface temperature for the example of 25 October. When the entire temperature profile was changed by +/- 2 K in the calculation of the right side of Equation (3), the resulting changes were very small; about 10 mb for  $P_c$  and 0.03 for  $NE$ . These errors are roughly inversely proportional to the lapse rate at the altitude of the cloud. When the surface temperature and the atmospheric temperature were adjusted by 5 and 2 K respectively, maximum errors of roughly 40 mb in  $P_c$  and 0.20 in  $NE$  were found for the situation where the surface temperature was underestimated and the atmospheric temperature was overestimated (perhaps possible in nearly clear sky with strong solar heating producing a very large lapse rate in the lower atmosphere). Where the surface temperature and the atmospheric temperature were both underestimated (possible in a warm frontal passage), the cloud was estimated to be too low in the atmosphere by 20 mb in  $P_c$  and too opaque by 0.10 in  $NE$ .

Experiments were also conducted simulating errors localized to only one level of the temperature profile. The results (not shown) were modified minimally. Little sensitivity is apparent for temperature errors low in the atmosphere ( $P_c > 700$ ), as expected from inspecting the transmittances of the MODIS CO<sub>2</sub> channels. An error of 2 C for a level between 700 and 300 mb can produce a shift of up to 30 mb in the cloud top pressure. This should be viewed in conjunction with the lapse rate of 5 C per 50 mb for the example of 25 October. Here and in other situations inspected, the errors in the CO<sub>2</sub> slicing cloud top pressure estimate,  $DP_c$ , caused by sounding errors,  $DT$ , in layers where the CO<sub>2</sub> spectral channels have sensitivity, are found to

be roughly inversely proportional to the lapse rate at the level of the cloud,  $L$ ; this can be expressed as  $DP_c = DT/L$ .

#### 3.1.3.a.6 Errors Associated with Instrument Noise

The VAS radiometer is accurate to better than  $1 \text{ mW/m}^2/\text{ster/cm}^{-1}$ . This corresponds to less than 1 K in the  $\text{CO}_2$  channels for temperatures ranging from 220 to 320 K. Noise affects the ability of the VAS to detect thin cirrus. Noise of 1 K implies that effective cloud emissivities of less than 10% cannot be resolved for high clouds (using  $D(NE) = DR / (R - R_{clr})$ ). In our earlier work of 1989, it was found that about half of the very thin clouds with  $NE$  less than 0.10 were classified incorrectly as low opaque cloud observations (this represented about 5% of all observations); it was also found that about half of these very thin clouds were correctly classified by the  $\text{CO}_2$  slicing algorithm.

The  $\text{CO}_2$  slicing technique cannot measure the properties of clouds where the contrast of radiation from cloud free and cloud obscured observations is too small for reliable discrimination in satellite  $\text{CO}_2$  spectral radiances (when radiance differences are less than  $.5 \text{ mW/m}^2/\text{ster/cm}^{-1}$  cloud properties are not calculated). This occurs for very thin cirrus (as discussed in the previous paragraph) and for some low clouds below 700 mb. Clouds below 700 mb were assumed to have an effective emissivity of one, thus preventing the interpretation of low broken cloud as cirrus. Occasionally, low clouds were also reported in situations of clear sky with tropospheric temperature inversions; this created problems in early morning statistics during the winter months.

When noise is introduced in one channel of the  $\text{CO}_2$  radiance ratio, the left side of Equation (3) changes. Using the example of 25 October once again, Figure 8 shows the noise induced changes in the ratio. The extremes produce a  $P_c$  that is 50 mb lower or make it impossible to have a solution in the atmosphere. This example is representative of further noise investigations in the  $\text{CO}_2$  slicing algorithm; the effect of sensor noise is typically less than 50 mb.

#### 3.1.3.a.7 Conclusions of the Cloud Top Pressure and Emissivity Error Studies

(i) Errors associated with the assumption of constant emissivity for the CO<sub>2</sub> channels are negligible.

(ii) The CO<sub>2</sub> slicing algorithm determines the height of the radiative center of the cloud; for optically thick clouds this is near the cloud top while for optically thin clouds it is near the cloud middle.

(iii) Multi-layer cloud situations where an opaque cloud underlies a transmissive cloud cause errors in the height of the transmissive cloud of about 100 mb for most cases (the cloud is determined to be too low in the atmosphere). The error in transmissive cloud height is largest when the underlying opaque layer is in the middle troposphere (400- 700 mb) and small to negligible when the opaque layer is near the surface or close to the transmissive layer.

(iv) When the surface temperature guess doesn't track surface warming (cooling), then the cloud layer is calculated to be too low (high). Nominal diurnal changes in the ground temperature are typically tracked to better than 5 C in the CO<sub>2</sub> slicing algorithm, so that they have little effect on the ability to detect transmissive clouds or to determine their heights.

(v) The CO<sub>2</sub> solution is largely insensitive to errors in the temperature sounding in the lower troposphere. There are often compensating effects in the integration of the atmospheric column. The errors in the CO<sub>2</sub> slicing cloud top pressure estimate caused by sounding errors in layers where the CO<sub>2</sub> spectral channels have sensitivity are roughly inversely proportional to the lapse rate at the level of the cloud.

(vi) Instrument noise causes the CO<sub>2</sub> slicing algorithm to miss roughly half of the thin cirrus with effective emissivity less than 0.10; this represents about 5% of all observations.

### 3.1.3.b Error Estimates of Cloud Phase Algorithm

Modeled results and observations of the infrared cloud phase determination suggest it is very reliable in the determination of low-level water clouds and high-level ice clouds with optical thicknesses above approximately 0.5. The most difficulty pertains to (a) midlevel clouds for which unambiguous cloud phase discrimination is problematic, (b) extremely optically thin cirrus, and (c) when thin cirrus overlies a lower-level cloud (i.e., multilayered clouds). Verification of cloud phase is being made through comparison of ER-2 based Cloud Lidar System (CLS) depolarization lidar with both MAS and MODIS data. Known sources of error are discussed below.

#### 3.1.3.b.1 Errors Due to Mixed Phase Cloud Scenes

Single-layered clouds of wide spatial extent having cloud-top temperatures in the range between 250K and 270K are prevalent in the storm tracks in both the Northern and Southern Hemispheres. Unambiguous phase discrimination for these clouds is extremely difficult. Current efforts are to improve cloud phase discrimination for clouds at temperatures between 233K and 273K, the range over which the presence of supercooled water is possible.

#### 3.1.3.b.2 Errors Due to Non-uniform Surface Emissivities

The current version of the bispectral technique assumes a uniform surface emissivity for both IR bands. This is certainly not the case for many different ground surface types, including bare soils and deserts. Gao and Wiscombe 1994 modeled the effects of different surface types on the BTD[8 – 11] values based on laboratory surface emissivity measurements. Their results suggest that certain types of bare rock, and dry vegetation lead to misidentification of cloud phase by the tri-spectral technique due the resultant location of the brightness temperatures differences on the scatter diagram. Many different MODIS and MAS data sets over numerous surface types have been investigated to date.

#### 3.1.3.b.3 Errors Due to Instrument Noise

An investigation into the effects of MAS pixel averaging on brightness temperature differencing was conducted, with distinct cloud signals becoming apparent after averaging over a 5 x 5 pixel box. This lowers the NEDT values for the 8, 11 and 12 micron channels (as evaluated for MAS 5 December 1993 data) to 0.13, 0.09 and 0.15 K respectively. The MODIS NEDT specifications of these infrared bands at 300 K is 0.05 K, suggesting that the noise is within the limits for cloud phase delineation.

### 3.2 Practical Considerations

#### 3.2.1.a Radiance Biases and Numerical Considerations of Cloud Top Properties Algorithm

The MODIS measured radiances have biases with respect to the forward calculated radiances using model estimates of the temperature and moisture profile for a given field of view. There are several possible causes for this bias: these include calibration errors, spectral response uncertainty, undetected cloud in the FOV, and model uncertainty. Solution of Equation (3) and (4) uses measured and calculated cloud forcing (clear minus cloudy FOV radiances) and thus requires that this bias be minimized. Techniques developed at the European Centre for Medium range Weather Forecast to characterize the HIRS radiance bias with respect to the ECMWF model (Eyre, 1992) are being employed in the MODIS cloud algorithm. In order to reduce systematic biases from being introduced into the cloud height calculations, simulated MODIS spectral radiances from clear-sky FOVs are compared to the corresponding observed radiances for several days at the beginning of each month processed. A regression relationship is developed for a correction to the simulated radiances during subsequent reprocessing of the data. One relationship is derived for ocean regions; another for land surface. (This is done automatically, with the radiances stored in a rotating file containing data from several previous days.)

The measured and the calculated radiance gradient ratios in Equation (3) do not always converge within the allowable pressure bounds (between the tropopause and the top of the inversion layer or the surface). Solutions are not accepted if found at the boundaries, even though there may be a good meteorological reason to accept these values. In these cases the opaque cloud solution from the window channel is used.

Evaluation of the integrals in the right side of Equation (3) or (3') are performed at 50 mb increments (the integration through the atmosphere is accomplished at discrete 50 mb intervals and the best pressure level interpolated to 10 mb). When the slope in Figure 8 increases, instrument noise causes more error in the cloud top pressure determination. It has been found that mid-latitudes have greater slopes than the tropics, thus cloud top pressures in the tropics might be slightly less error prone.

### 3.2.1.b Numerical Considerations of Cloud Phase Algorithm

The implementation of the cloud phase algorithm is very straightforward, and requires that the cloud mask product (MOD35) be available as well as the 8.5 and 11- $\mu\text{m}$  BT's for each cloudy pixel.

### 3.2.2.a Programming Considerations of Cloud Top Properties Algorithm

Processing is accomplished for every 5 x 5 pixel area (5 km resolution at nadir). The clear sky radiances come from a spatial analyses of the pixels designated clear by the cloud mask. Spatial registration of the channels must occur, so that FOVs can be collocated with ancillary data.

The CO<sub>2</sub> slicing algorithm has been used for the past nine years on VAS data over North America and for the past seven years on global HIRS data. It is a robust algorithm. The census of cirrus clouds derived from both of these efforts has been published in refereed literature.

Processing time for the MOD06CT algorithm are derived from using the direct broadcast version on a Sun solarix x86 machine. To process 5000 lines (~10 minutes) requires ~ 15 minutes.

The product Level 2 MOD06CT-5km volume per granule (5 minutes of data) is 14 MB. A full day of MODIS processing results in a volume load of 14 MB/granule \* 288 granules/day = 4.0 GB/day for the parameters listed in Table 5. It should be noted that product MOD06 also includes particle radius and optical thickness retrievals at 1km during the daytime. This increase the size of daytime granules to 60 MB.

### 3.2.3. Validation

Validation is being approached in several ways: (i) collocation with higher resolution aircraft data, (ii) ground-based and aircraft in situ observations, and (iii) intercomparisons with other AM-1 platform instruments. Our validation approach relies heavily on the sources of the data that were used in the algorithm development, which consisted primarily of the MAS, a fifty channel visible, near-infrared, and thermal infrared imaging spectrometer with 50 m resolution at nadir (cf. King et al. 1996), HIS, a 2 km resolution nadir-viewing Michelson interferometer (later replaced by SHIS, a scanning version) with 0.5 cm<sup>-1</sup> spectral resolution from 4 to 15 μm (Revercomb et al. 1988), AVIRIS, a 224 band imaging spectrometer from 0.4-2.5 μm with 20 m resolution at nadir, and CPL, a dual polarization nadir viewing lidar (McGill et al. 2002).

Well-calibrated radiances are essential for the development of accurate algorithms. The calibration of the HIS is such that it serves as a reference for line-by-line radiative transfer models. The MAS infrared channels are calibrated through two onboard blackbody sources that

are viewed once every scan. Calibration of the shortwave infrared and thermal infrared channels is routinely assessed through vicarious calibration and intercomparisons with the HIS flying on the same aircraft. The MAS solar channels are calibrated in the laboratory, using a 30" integrating sphere before and after each ER-2 deployment, as well as a 20" integrating hemisphere shipped to the field deployment site for calibration trending during deployments. A comprehensive description of both the shortwave and longwave calibration procedures, signal-to-noise characteristics, and thermal vacuum characterization of the MAS can be found in King et al. (1996).

Several field campaigns were planned with the ER-2 aircraft carrying the MAS and HIS (later, SHIS) over various scenes and ecosystems. In addition to the major national and international activities outlined above, we led several focused and short field deployments:

- cold season deployments over the Great Lakes, Hudson Bay, sea ice, and lake ice (based in Madison, WI);
- warm season deployments over the Gulf of Mexico, ARM CART, mountains, and desert (based in Texas or California).

For ARM CART site missions, ground based measurements were included in the data collection. This entailed deployment of the MAS and HIS (SHIS) on the ER-2 aircraft to coincide with a MODIS overflight and to collect simultaneous ground-based class-sondes, AERI (a ground-based Michelson interferometer), tower measurements of temperature and moisture at various elevations, microwave moisture measurements, lidar and radar cloud observations, and whole sky camera images.

Comparisons with products from other platforms have also been made. Cloud masks have been compared with those from AVHRR and HIRS/2 data, ASTER and MISR (also on the AM-1 platform), and CERES. Atmospheric profiles have been compared with those from HIRS, GOES, and AIRS (also on the PM-1 platform). Cloud properties have been intercompared with those derived from HIRS, GOES, CERES, MISR and AIRS, as well as from in situ aircraft (see below). Timing, coverage and resolution vary from one instrument to another; for example with ASTER, comparisons are possible for selected swaths (60 km wide with 30 m resolution) that are available for different (and selected) ecosystems no more than once every 16 days.

#### **Table 4. MODIS Field Campaigns used in Cloud Properties Validation**

<i>Mission</i>	<i>Dates</i>	<i>Responsible Team Members</i>	<i>Primary Purpose</i>
SUCCESS	April-May 1996	Si-Chee Tsay, Steve Ackerman, Steve Platnick	cirrus cloud properties with MAS and HIS
WINCE	February 1997	Paul Menzel, Steve Ackerman, Dorothy Hall	cloud detection and properties over snow/ice covered land and lakes with MAS and HIS
FIRE III	April-June 1998 August 1998	Michael King Si-Chee Tsay	arctic stratus clouds over sea ice with MAS, HIS
WINTEX	March 1999	Paul Menzel, Steve Ackerman, Bill Smith	atmospheric sounding and cloud/snow detection in winter MAS, SHIS, NAST
WISC-T2000	March 2000	Paul Menzel, Steve Ackerman	First assessment of Terra MODIS radiometric performance with MAS, SHIS, CPL
TX-2001	March – April 2001	Paul Menzel, Steve Ackerman	Radiometric assessment of Terra MODIS with MAS, SHIS
TX-2002	November – December 2002	Paul Menzel, Steve Ackerman	LIB and Cloud properties assessment of Terra and Aqua MODIS with MAS, SHIS, and CPL
Thorpex PTOST	February-March 2003	Steve Ackerman, John Murray, Bill Smith	Atmospheric profiles, cloud properties for Aqua MODIS with MAS, SHIS, NAST, CPL

Several field programs have already offered opportunities for pre-launch and post-launch MODIS validation through collection and analysis of observations obtained from MAS, HIS (SHIS), NAST, and CPL. Those field campaigns relating primarily to cloud top properties and cloud phase are found in Table 4.

The Subsonic Aircraft Contrail and Cloud Effects Special Study (SUCCESS) field experiment in April-May 1996 had the goal of determining the radiative properties of cirrus contrails, and to contrast them with naturally occurring cirrus. To assess the radiative impact of these clouds requires a well-calibrated set of radiation measurements and “ground (or in situ) truth” observations. During SUCCESS several MAS and HIS multispectral observations from the NASA ER-2 aircraft were coordinated with in situ aircraft and ground based measurements. The MAS and HIS measurements address the very important relationship between cirrus radiative properties and the thermodynamic environment (atmospheric temperature and moisture conditions) wherein cirrus clouds form and are maintained. The HIS provides accurate measurements of the atmospheric thermodynamical properties supporting the cirrus life cycle and the MAS measures the cirrus areal extent and radiative properties. Special emphasis has



been placed on developing and validating methods of detecting upper tropospheric clouds and defining their areal extent with infrared (e.g. 13.9  $\mu\text{m}$ ) and near infrared (e.g. 1.88  $\mu\text{m}$ ) channels; these are similar to the MODIS channels and MAS cirrus detection has direct relevance to the MODIS cloud mask algorithm.

Several studies have demonstrated the sensitivity of spectral radiances to cloud particle size and shape distributions. The MAS and HIS instruments provide accurate spectral measurements that can be used to assess differences in the radiative signatures between contrails and naturally occurring cirrus clouds. One difficulty in assessing the impact of high-altitude subsonic aircraft on cirrus formation and modification is the natural variability of the atmosphere and the potentially small signal of the radiative perturbation. Variations in the atmospheric spectral properties for contrail and natural cirrus conditions have been assessed with the two ER-2 instruments in conjunction with in situ and ground-based observations.

The Winter Cloud Experiment (WINCE January-February 1997) was a first investigation into the difficulties of detecting cloud and estimating their properties in winter conditions. Cirrus and thin clouds over frozen tundra and lakes in the northern USA and Canada were measured with the MAS and HIS (along with the GOES-8 and AVHRR). One of the missions investigated the product stability in the transition from day (visible plus infrared) to night (infrared only) and then nighttime only. In addition two ground sites in New England were instrumented for snow and ice cover measurements and MAS/HIS flights were made in clear sky condition (in collaboration with Dorothy Hall and George Riggs working on the MODIS snow/ice product). The field campaign centered in Madison. Examples of the MAS cloud mask were distributed to science team members.

FIRE, the First ISCCP (International Satellite Cloud Climatology Project) Regional Experiment, has previously conducted four successful field missions focused on cloud remote sensing and modeling studies as they relate to climate. FIRE Phase III was conducted in the Arctic in two phases, phase I to be conducted over a 7 week period or longer with a serial deployment of low- to mid-level aircraft, together with a 4 week period of high-altitude ER-2 overflights. During this component of FIRE III, the University of Washington CV-580 and, to a lesser extent, the NCAR C-130Q were utilized. Both of these aircraft were equipped with an extensive set of PMS cloud microphysics probes, a Gerber PVM-100A liquid water content and effective radius probe, Johnson-Williams and King hot wire probes, a Nd:YAG lidar,

thermodynamic state variable measurements, and selected chemistry instrumentation. In addition, the ER-2 participated as the upper level aircraft from May 18-June 9, with the MAS, HIS, CLS lidar, a radiation measurement system for radiative fluxes, a multispectral along-track scanning radiometer, and a microwave imaging radiometer. The primary sensors of interest to Goddard Space Flight Center (Michael King, Si-Chee Tsay, Steve Platnick, Robert Pincus) are the MAS on the ER-2, the CAR on the CV-580, and numerous in situ microphysics probes that are invaluable in accessing the accuracy of cloud retrievals of the microphysical and radiative properties of Arctic stratus clouds over a bright (sea ice) surface. This valuable data set has also been of interest to the University of Wisconsin for testing the cloud mask algorithm, cloud phase and cloud top properties.

The first EOS-targeted campaign after the Terra MODIS launch was the WISC-T2000 field campaign. During WISC-T2000, the ER-2 overflew clear scenes of the Great Lakes for L1B validation, and cloudy scenes for cloud properties and cloud detection both in the upper Midwest and over the ARM CART site in Oklahoma. The ER-2 with MAS, SHIS, and CPL were deployed to synchronize with the MODIS overflight; the ARM site suite of ground-based measurements (class-sonde, AERI, tower measurements of temperature and moisture at various elevations, microwave moisture measurements, lidar and radar observations, whole sky images) were collected simultaneously. These measurements were useful to obtain a first assessment of MODIS radiance measurements and geophysical parameters as well. Lidar and radar observations of cloud boundaries over the ARM sites are useful to validate the presence of a cloud as well as its cloud top pressure altitude. Whole sky imagers were also available at the site to compare satellite and ground-based estimates of cloud amount. Finally, optical depth measurements derived from lidar aid in specifying the limit of thin cirrus detection in the cloud mask algorithm and for cloud properties.

The TX-2001 field campaign was designed to do an indepth assessment of Terra MODIS L1B radiometric performance. This effort collected simultaneous MODIS and MAS, SHIS data over clear scenes of the Gulf of Mexico. Targets were selected to include different scan angles from Terra so that insight could be gained on MODIS scan mirror characterization. This effort showed that the MODIS LWIR cloud phase bands at 8.6um 11um and 12um were indeed well calibrated, complementing first such results from the SAFARI-2000 field program. TX-2001 also showed that the LWIR CO2 bands were however performing too warm, launching an effort

that ultimately resulted in an adjustment to the radiometry of these bands for the cloud top properties algorithm.

The TX-2002 field program utilized the MAS, SHIS, NAST, and CPL instruments on the ER-2 for assessing the Aqua MODIS L1B radiometric performance and for assessing the Terra MODIS cloud properties products. Flights over the Gulf of Mexico were used for L1B validation and cloud products assessment. The ER-2 also overflew the ARM CART site in Oklahoma with simultaneous ground based lidar and other ground based instrumentation. These data sets first demonstrated the high quality of Aqua MODIS L1B radiometric performance; however they showed that the LWIR CO<sub>2</sub> bands on Aqua also were warmer than expected. The data collection also showed that the Terra MODIS cloud top pressure retrievals tended to be too low in the atmosphere, an important confirmation that continues to be used.

The THORPEX PTOST field effort took place out of Hawaii in February-March 2003 with the MAS, SHIS, CPL, and NAST instruments on the ER-2. These flights were targeted towards validating Aqua MODIS cloud products as well as early GLAS performance. High quality data sets over the Pacific Ocean for a wide range of cloud conditions (single layer thin and thick, multilayer, mid layer, mixed phase, etc.) made this one of the richest data sets collected for cloud product assessment. These data sets have been used to demonstrate that adjustments to the cloud properties algorithms improved the cloud height estimates. The data set also gave a first look into the performance of the cloud phase algorithm, particularly in the challenging environment of mixed phase clouds.

An independent ground validation campaign of MODIS cloud heights is being undertaken through comparisons with stereo determinations of cloud heights (using the MISR over Great Britain and two GOES satellites over the U. S.), aircraft reports of cirrus cloud heights (from the ACARS), and lidar estimates of cirrus heights (using the University of Wisconsin lidar). These intercomparisons have led to useful comparisons between MISR and MODIS cloud detection and cloud heights. Validation of the MODIS cloud emissivity is being attempted through comparison with the lidar determinations. Pre-launch validations came from cloud top property determinations with MAS data from several field campaigns which included lidar measurements.

Other field campaigns reaching outside the scope of the cloud properties have been conducted. These supply useful data at times for cloud product assessment, particularly when

these campaigns are conducted in different environments/climate regions of the World. Table 5 shows some of these. This indicates the intention for an ongoing Cal / Val activity.

<b>Table 5: Calibration and Validation Field Campaigns</b>			
<b>Name</b>	<b>Reference URL</b>	<b>Principal Airborne Sensors</b>	<b>Primary Purpose</b>
SAFARI-2000	<a href="http://safari.gecp.virginia.edu">safari.gecp.virginia.edu</a>	MAS, SHIS, CPL, AirMISR	Biophysical validation, LST, VI, Albedo, Aerosol, Fire
BOREAS	<a href="http://boreas.gsfc.nasa.gov/html_pages/boreas_home.html">boreas.gsfc.nasa.gov/html_pages/boreas_home.html</a>		Biophysical validation, LST, VI, Albedo, Aerosol, Fire
LBA	<a href="http://www-eosdis.ornl.gov/lba_cpctec/indexi.html">www-eosdis.ornl.gov/lba_cpctec/indexi.html</a>	MAS	Biophysical validation, LST, VI, Albedo, Aerosol, Fire
CLAMS	<a href="http://snowdog.larc.nasa.gov/cave/cave2.0/C/LAMS.dir/index.html">snowdog.larc.nasa.gov/cave/cave2.0/C/LAMS.dir/index.html</a>	NAST-I, NAST-M, MAS	Aerosols
CRYSTAL		MAS, SHIS, NAST, CPL	4-D water vapor fields. Convective initiation. Cirrus particle properties
THORPEX ATOST	<a href="http://www.nrlmry.navy.mil/~langland/THORPEX_document/Thorpex_plan.htm">www.nrlmry.navy.mil/~langland/THORPEX_document/Thorpex_plan.htm</a>	MAS, SHIS, NAST, CPL	Atmospheric water vapor and atmospheric turbulence associated with jet streaks
CAMEX	<a href="http://ghrc.msfc.nasa.gov/camex3/instruments/lase.html">ghrc.msfc.nasa.gov/camex3/instruments/lase.html</a>	MAMS, EDOP	Tropical storm structure
ACE-1 ACE-2	<a href="http://saga.pmel.noaa.gov/ace1.html">saga.pmel.noaa.gov/ace1.html</a> <a href="http://www.ei.jrc.it/ace2">www.ei.jrc.it/ace2</a>		Aerosol, dust transport, RTE

### 3.2.3.a Validation of Cloud Top Properties Algorithm

The CO<sub>2</sub> slicing algorithm uses calibrated radiances that are bias adjusted with respect to the NCEP forward calculations of clear sky radiances. Also the algorithm depends on the spectral radiance gradients or cloud forcing (clear minus cloudy fov radiances). These two considerations mitigate the algorithm dependence on extremely accurate calibration, although it is highly desirable.

As outlined in section 3.2.3 above, validation of the MODIS cloud heights is being undertaken through comparisons with stereo determinations of cloud heights (using the two GOES satellites over the U. S. and the University of Chicago ground all sky cameras), estimates of cloud height from cloud shadows, (using aircraft MAS, NOAA AVHRR, and GOES data), reports of cirrus cloud heights (from the ACARS), and lidar estimates of cirrus heights (using the University of Wisconsin lidar). These intercomparisons are being conducted in concert with

field campaigns of the MAS on the ER-2 after MODIS launch. Validation of the MODIS cloud emissivity is being attempted through comparison with the lidar determinations. Pre-launch validations came from cloud top property determinations with MAS data from several field campaigns which included stereo and lidar measurements also.

Post-launch validation was made by comparing the cloud top properties product with CERES single sample footprint (SSF) and single satellite gridded (SSG) products that include cloud top pressure and temperature. CERES is heavily dependent on MODIS observations for cloud detection, so it is important to ensure that the MODIS and CERES-derived cloud products are consistent. MISR altitude binned cloud fraction and stereo heights are being compared with the MODIS effective emissivity and cloud top heights to geometrically validate the MODIS radiometrically derived cloud height data.

#### 3.2.3.b Validation for Cloud Phase Algorithm

The cloud phase algorithm uses calibrated radiances converted into brightness temperatures, and averaged over a 5 x 5 pixel box. The use of temperature differences between the 8, 11, and 12 micron channels averaging also stresses the algorithm dependence on very accurate relative calibration between channels.

Validation of the infrared cloud thermodynamic phase product is made primarily through comparisons with cloud lidar determinations (CLS onboard the ER-2) and cloud microphysical data (collected on instruments onboard the CV-580 and NCAR C-130Q) collected during field campaigns outlined in section 3.2.3 above. Limited pre- and post-launch validation was carried out using collocated HIRS/AVHRR data sets, focusing on surface emissivity effects. This data set has the advantage of its global coverage, but the spatial scale is far removed from that of MODIS, and the spectral bandwidths are wider and off center from those of MODIS. Post-launch validation consists of close inspection of sections of data representing differing cloud regimes and surface types, including cross checks during the day mode with the visible reflection function technique of King et al. (ATBD-MOD-05) and consistency with the cloud top properties results. Finally, post-launch validation includes intercomparisons with other EOS instrument products such as the CERES SSF and SSG cloud phase product, and the ASTER polar cloud mask product, which includes a cloud phase bit.

#### 3.2.4.a Quality Control of Cloud Top Properties Algorithm

As indicated in section 3.1.3.a., the accuracy of the cloud top pressures have been found to be 50 mb root mean square with respect to radiosonde, stereo, and lidar estimates; the effective emissivity determinations have been found to be correlate within 20% root mean square of lidar visible estimates of optical thickness.

Quality control within the software checks for cloud forcing greater than the instrument noise and cloud top pressure within the atmospheric layer where temperature and pressure enjoy a one to one relationship. Additionally, cloud top pressures are stratified as a function of satellite viewing angle to make sure that the atmospheric transmittance corrections for viewing angle are not introducing a bias.

Beyond these simple tests, quality control is accomplished by manual and automated inspection of the data and comparison to other sources of cloud information. MODIS cloud top pressures and effective emissivities are being compared to those determined from the NOAA HIRS and the GOES sounder. Additional data from field experiments using the MODIS Airborne Simulator on the ER2 assists with quality assessment of the MODIS cloud parameter determinations.

Global mean distributions of cloud height and emissivity are being compared from one week to the next; thresholds are set to flag unrealistic changes. Trend analyses of global cloud properties are being compared with trends in OLR; a strong correlation between the two is being realized. Additionally comparisons with ISSCP are being made. These comparisons are all done with the gridded 1.0 degree resolution MODIS cloud properties (determined from averaging of the 5 x 5 pixel cloud properties).

The cloud top properties and cloud phase product (the 5 km resolution part of MOD06) carry 10 bytes of quality analysis information for each pixel. The information contained in this byte array include a confidence in the usefulness of each individual parameter, input data resource flags and processing path flags. Please refer to the MODIS Atmosphere QA Plan for exact details.

#### 3.2.4.b Quality Control of Cloud Phase Algorithm

Quality control includes consistency checks with previous days resultant statistics, including the global cloud phase determination consistency and known cloud area persistence consistency (marine stratus regions, etc.).

The cloud top properties and cloud phase product (the 5 km resolution part of MOD06) carry 10 bytes of quality analysis information for each pixel. The information contained in this byte array include a confidence in the usefulness of each individual parameter, input data resource flags and processing path flags. Please refer to the MODIS Atmosphere QA Plan for exact details.

### 3.2.5 Exception Handling

If the required radiance data is not available, then the algorithm records the cloud products missing for that 5 x 5 pixel area.

#### 3.2.6.a Data Dependencies of Cloud Top Properties Algorithm

The CO<sub>2</sub> slicing algorithm needs calibrated, navigated, coregistered one km FOV radiances from channels 29 (8.6 micron for moisture correction), 31 (11.03 micron infrared window), 32 (12.02 micron for moisture correction), 33-36 (13.335, 13.635, 13.935, and 14.235 microns CO<sub>2</sub> absorption band channels). Navigation implies knowledge of the surface terrain including height (DEM) and whether land or sea. The MODIS viewing angle for a given FOV must be known. The cloud mask from visible and infrared radiance considerations is used as a indicator for cloud cover within a given one km FOV. The NCEP GDAS Final Run global model analysis of surface temperature and pressure as well as profiles of temperature and moisture are initially used in the calculation of the cloud forcing as a function of pressure and effective emissivity (in Equation (3)); AIRS/AMSU profiles are also used. The Reynolds blended SST is also used over the ocean. The algorithm also requires knowledge of the clear radiances for evaluation of the cloud forcing for each channel used in the ratio tests. This information is provided in the form of clear radiance maps created and updated daily by the cloud mask production software. Table 6 summarizes the input data dependencies.

There has been some consideration for using the short wavelength CO<sub>2</sub> spectral bands 22 through 25 in parallel with the long wavelength CO<sub>2</sub> bands in a composite CO<sub>2</sub> slicing algorithm. The shortwave CO<sub>2</sub> algorithm has problems with reflected solar contributions during daylight

hours, but is useful additional information at night. Current plans do not include these bands, but future versions of the software might.

---

**Table 6. MODIS Cloud Parameter Input Data Dependencies**

MODIS data channels	29, 31-36
Navigation	lat, lon, land, sea
MODIS viewing angle	lin, ele, ang
Cloud mask	yes, no, type
Surface data	SST, model analysis of temperature, dewpoint and pressure,
Model profiles	topography (DEM) temp (12 levels), moisture (6 levels)
Clear Radiance Base Maps	Channels 31, 33-36.

---

3.2.6.a Data Dependencies of Cloud Phase Algorithm

The bispectral cloud phase algorithm needs calibrated, navigated, coregistered one km FOV radiances (for FOV uniformity screening and conversion to brightness temperatures) from channels 29 (8.6 micron) and 31 (11.03 micron). The MODIS viewing angle for a given FOV must be known. The MODIS cloud mask product is used to screen areas where the probability of cloud is high. A global surface emissivity map (related to surface cover) is used to adjust ice/water thresholds. Table 7 is a summary of the input data dependencies.

---

**Table 7. MODIS Cloud Phase Input Data Dependencies**

MODIS data channels	29, 31
MODIS cloud mask	cloud or clear
Navigation	lat, lon, land, sea
MODIS viewing angle	lin, ele, ang
Surface data	surface emissivity

---

3.2.7.a Level 2 Output Product of Cloud Top Properties and Cloud Phase Algorithm

The Level 2 output file for each 5 x 5 pixel area (when cloud is present) is summarized in Table 8. The combined MODIS cloud properties, cloud phase and cloud retrieval product number is MOD06.



---

**Table 8. MODIS cloud product (MOD06 - 5 km) Output File Contents**

parameter type	Bytes	content
double	8	Scan Start Time
float	4	location latitude
float	4	location longitude
short	2	Solar Zenith Angle
short	2	Solar Azimuth Angle
short	2	Sensor Zenith Angle
short	2	Sensor Azimuth Angle
short	14	brightness temperature of bands 29,31-36
short	2	surface temperature
short	2	surface pressure
byte	1	processing flag
byte	1	cloud height method (CO <sub>2</sub> slicing or IR window)
short	2	cloud top pressure
short	2	cloud top pressure day
short	2	cloud top pressure night
short	2	cloud top temperature
short	2	cloud top temperature day
short	2	cloud top temperature night
short	2	tropopause height
byte	1	cloud fraction
byte	1	cloud fraction day
byte	1	cloud fraction night
byte	1	cloud effective emissivity
byte	1	cloud effective emissivity day
byte	1	cloud effective emissivity night
short	2	cloud top pressure from IR window
short	2	spectral cloud forcing
short	10	cloud top pressure from ratios (33/31, 34/33, 35/33, 35/34, 36/35)
short	2	surface type
short	14	radiance variance (7 channels)
short	4	brightness temperature difference (8-11, 11-12)
byte	1	cloud phase infrared
byte	1	cloud phase infrared day
byte	1	cloud phase infrared night
byte	10	quality assurance at 5x5 km resolution

Total: 111 bytes/pixel

---

### 3.2.7.b Level 3 Output Product of Cloud Top Properties and Cloud Phase Algorithm

The Level 3 cloud top properties and cloud phase products are included as part of a joint atmosphere discipline group product (MOD44). The products are produced on a daily bases from the Level 2 files, on an 8 day basis from the daily files and a monthly bases from the daily Level 3 files. The Level 3 daily files are produced at 1.0 degree equal area only, while the 8 day and monthly Level 3 product files are produced for both 1.0 degree equal area and 1.0 degree equal angle grids. The cloud top properties and cloud phase contribution to the joint product is shown in Table 9. An example of the probability of cirrus equal angle Level 3 product derived from MODIS data is provided in Figure 10.

---

**Table 9. Cloud Top Property and Cloud Phase Level 3 Output File Contribution to Joint Atmosphere Level 3 Products**

parameter number	content
1	thermodynamic phase (coded 0-6)
2	thermodynamic phase (coded 0-6) day
3	thermodynamic phase (coded 0-6) night
4	cloud top temperature
5	cloud top temperature day
6	cloud top temperature night
7	cloud top pressure
8	cloud top pressure day
9	cloud top pressure night
10	cloud top effective emissivity
11	cloud top effective emissivity day
12	cloud top effective emissivity night
13	probability of cirrus
14	probability of high cloud

---

### 3.3 References for sections 2 and 3.

Ackerman, S. A., W. L. Smith and H. E. Revercomb, 1990: The 27-28 October 1986 FIRE IFO cirrus case study: spectral properties of cirrus clouds in the 8-12 micron window. Mon. Wea. Rev., 118, 2377-2388.

- Baum, B. A., D. P. Kratz, P. Yang, S. Ou, Y. Hu, P. F. Soulen, and S-C. Tsay, 2000a: Remote sensing of cloud properties using MODIS Airborne Simulator imagery during SUCCESS. I. Data and models. *J. Geophys. Res.*, **105**, 11,767-11,780.
- Baum, B. A., P. F. Soulen, K. I. Strabala, M. D. King, S. A. Ackerman, W. P. Menzel, and P. Yang, 2000b: Remote sensing of cloud properties using MODIS Airborne Simulator imagery during SUCCESS. II. Cloud thermodynamic phase. *J. Geophys. Res.*, **105**, 11,781-11,792.
- Baum, B. A., A. J. Heymsfield, P. Yang, and S. T. Bedka, 2005a: Bulk scattering models for the remote sensing of ice clouds. Part 1: Microphysical data and models. *J. Appl. Meteor.*, **44**, 1885-1895.
- Baum, B. A., P. Yang, A. J. Heymsfield, S. Platnick, M. D. King, and S. T. Bedka, 2005b: Bulk scattering models for the remote sensing of ice clouds. Part 2: Narrowband models. *J. Appl. Meteor.*, **44**, 1896-1911.
- Booth, A. L., 1973: Objective cloud type classification using visual and infrared satellite data. 3rd Conference on Probability and Statistics in the Atmospheric Sciences. Am. Meteor. Soc., Boulder, CO.
- Chahine, M. T., 1974: Remote sounding of cloudy atmospheres. I. The single cloud layer. *J. Atmos. Sci.*, **31**, 233-243.
- Downing, H. D., and D. Williams, Optical constants of water in the infrared, *J. Geophys. Res.*, **80**, 1656-1661, 1975.
- Eyre, J. R., and W. P. Menzel, 1989: Retrieval of cloud parameters from satellite sounder data: A simulation study. *J. Appl. Meteor.*, **28**, 267-275.
- Gao, B.-C. and W. J. Wiscombe, 1994: Surface-induced brightness temperature variations and their effects on detecting thin cirrus clouds using IR emission channels in the 8-12 micron region. *J. Appl. Met.*, **33**, 568-570.
- Gruber, A., and T. S. Chen, 1988: Diurnal variation of outgoing longwave radiation. *J. Clim. Appl. Meteor.*, **8**, 1-16.
- Heymsfield, A. J., A. Bansemer, P. R. Field, S. L. Durden, J. Stith, J. E. Dye, W. Hall, and T. Grainger, 2002: Observations and parameterizations of particle size distributions in deep tropical cirrus and stratiform precipitating clouds: Results from in situ observations in TRMM field campaigns. *J. Atmos. Sci.*, **59**, 3457-3491.

- Inoue, T., 1987: A cloud type classification with NOAA 7 split window measurements. *J. Geophys. Res.*, **92**, 3991-4000.
- Inoue, T., 1989: Features of clouds over the Tropical Pacific during the Northern Hemispheric winter derived from split window measurements. *J. Meteor. Soc. Japan*, **67**, 621-637.
- Jacobowitz, H. J., 1970: Emission scattering and absorption of radiation in cirrus clouds. Ph.D. thesis, Massachusetts Institute of Technology, 181 pp.
- King, M. D., W. P. Menzel, P. S. Grant, J. S. Myers, G. T. Arnold, S. E. Platnick, L. E. Gumley, S. C. Tsay, C. C. Moeller, M. Fitzgerald, K. S. Brown and F. G. Osterwisch, 1996: Airborne scanning spectrometer for remote sensing of cloud, aerosol, water vapor and surface properties. *J. Atmos. Oceanic Technol.*, **13**, 777-794.
- King, M. D., Y. J. Kaufman, W. P. Menzel and D. Tanre, 1992: Remote sensing of cloud, aerosol, and water vapor properties from the Moderate Resolution Imaging Spectrometer (MODIS). *IEEE Trans. Geosci. Remote Sensing*, **30**, 2-27.
- Kratz, D. P., 1995: The correlated k-distribution technique as applied to the AVHRR channels, *J. Quant. Spectrosc. Radiat. Transfer*, **53**, 501-517.
- Kratz, D. P., and F. G. Rose, 1999: Accounting for the molecular absorption within the spectral range of the CERES window band, *J. Quant. Spectrosc. Radiat. Transfer*, **61**, 83-95.
- McGill, M.J., D.L. Hlavka, W.D. Hart, J.D. Spinhirne, V.S. Scott, and B. Schmid, "The Cloud Physics Lidar: Instrument description and initial measurement results", *Applied Optics*, **41**, pg. 3725-3734, June 2002.
- Menzel, W. P., W. L. Smith, and T. R. Stewart, 1983: Improved cloud motion wind vector and altitude assignment using VAS. *J. Clim. Appl. Meteor.*, **22**, 377-384.
- Menzel, W. P., D. P. Wylie, and A. H.-L. Huang, 1986: Cloud top pressures and amounts using HIRS CO<sub>2</sub> channel radiances. Technical Proceedings of the Third International TOVS Study Conference, 13-19 August 1986, Madison, WI, 173-185.
- Menzel, W. P. and K. I. Strabala, 1989: Preliminary report on the demonstration of the VAS CO<sub>2</sub> cloud parameters (cover, height, and amount) in support of the Automated Surface Observing System (ASOS). NOAA Tech Memo NESDIS 29.
- Menzel, W. P., D. P. Wylie, and K. I. Strabala, 1989: Characteristics of global cloud cover derived from multispectral HIRS observations. Technical Proceedings of the Fifth International TOVS Study Conference, 24-28 July 1989, Toulouse, France, 276-290.

- Menzel, W. P., D. P. Wylie, and K. I. Strabala, 1992: Seasonal and Diurnal Changes in Cirrus Clouds as seen in Four Years of Observations with the VAS. *J. Appl. Meteor.*, 31, 370-385.
- Parol, F. J., C. Buriez, G. Brogniez and Y. Fouquart, 1991: Information content of AVHRR Channels 4 and 5 with respect to the effective radius of cirrus cloud particles. *J. Appl. Meteor.*, 30, 973-984.
- Rossow, W. B., and A. A. Lacis, 1990: Global and seasonal cloud variations from satellite radiance measurements. Part II: Cloud properties and radiative effects. *J. Clim.*, in press.
- Smith, W. L., H. M. Woolf, P. G. Abel, C. M. Hayden, M. Chalfant, and N. Grody, 1974: Nimbus 5 sounder data processing system. Part I: Measurement characteristics and data reduction procedures. NOAA Tech. Memo. NESS 57, 99pp.
- Smith, W. L., and C. M. R. Platt, 1978: Intercomparison of radiosonde, ground based laser, and satellite deduced cloud heights. *J. Appl. Meteor.*, 17, 1796-1802.
- Smith, W. L., H. M. Woolf, and H. E. Revercomb, 1991: Linear simultaneous solution of temperature and absorbing constituent profiles from radiance spectra. *Appl. Optics*, 30, 1117-1123.
- Spinhirne, J.D., and W. D. Hart, 1990: Cirrus structure and radiative properties from airborne lidar and spectral radiometer observations. *Mon. Wea. Rev.*, 2329.
- Strabala, K. I., S. A. Ackerman and W. P. Menzel, 1994: Cloud properties inferred from 8-12 micron data. Accepted to the *J. Appl. Meteor.*, March 1994 issue.
- Susskind, J., D. Reuter, and M. T. Chahine, 1987: Cloud fields retrieved from analysis of HIRS/MSU sounding data. *J. Geophys. Res.*, 92, 4035-4050.
- Takano, Y., K. N. Liou and P. Minnis, 1992: The effects of small ice crystals on cirrus infrared radiative properties. *J. Atmos. Sci.*, 49, 1487-1493.
- Warren, S. G., 1984: Optical constants of ice from the ultraviolet to the microwave. *Appl. Optics*, 23, 1206-1225.
- Wielicki, B. A., and J. A. Coakley, 1981: Cloud retrieval using infrared sounder data: Error analysis. *J. Appl. Meteor.*, 20, 157-169.
- Wu, M. L. and J. Susskind, 1990: Outgoing longwave radiation computed from HIRS2/MSU soundings. *J. Geophys. Res.*, 95D, 7579-7602.

- Wylie, D. P., and W. P. Menzel, 1989: Two years of cloud cover statistics using VAS. *J. Clim.*, 2, 380-392.
- Wylie, D. P. and W. P. Menzel, 1991: Two Years of Global Cirrus Cloud Statistics using HIRS. Technical Proceedings of the Sixth International TOVS Study Conference held 1-6 May 1991 in Airlie, VA, 344-353.
- Wylie, D. P., W. P. Menzel, H. M. Woolf, and K. I. Strabala, 1994: Four Years of Global Cirrus Cloud Statistics Using HIRS. *J. Clim.*, 7, 1972-1986.
- Zhang, H. and W. P. Menzel, 2002: Improvement in Thin Cirrus Retrievals Using an Emissivity Adjusted CO<sub>2</sub> Slicing Algorithm. Accepted by *Jour. Geophys. Rev.*

#### **4.0 Assumptions**

##### **4.0.a Assumptions of Cloud Top Properties Algorithm**

The data is assumed to be calibrated (within the instrument noise), navigated (within one FOV), and coregistered (within two tenths of a FOV). The algorithm assumes the presence of only one cloud layer of infinitesimal thickness; adjustments for the presence of multiple cloud layers are under investigation. The cloud need not cover the entire FOV. Spectral cloud forcing must be greater than the instrument noise. Bias between global forecast model calculated and MODIS measured radiances must be accounted for.

##### **4.0.b Assumptions of Cloud Phase Algorithm**

Assumptions are discussed in the estimate of error section 3.1.3.b.

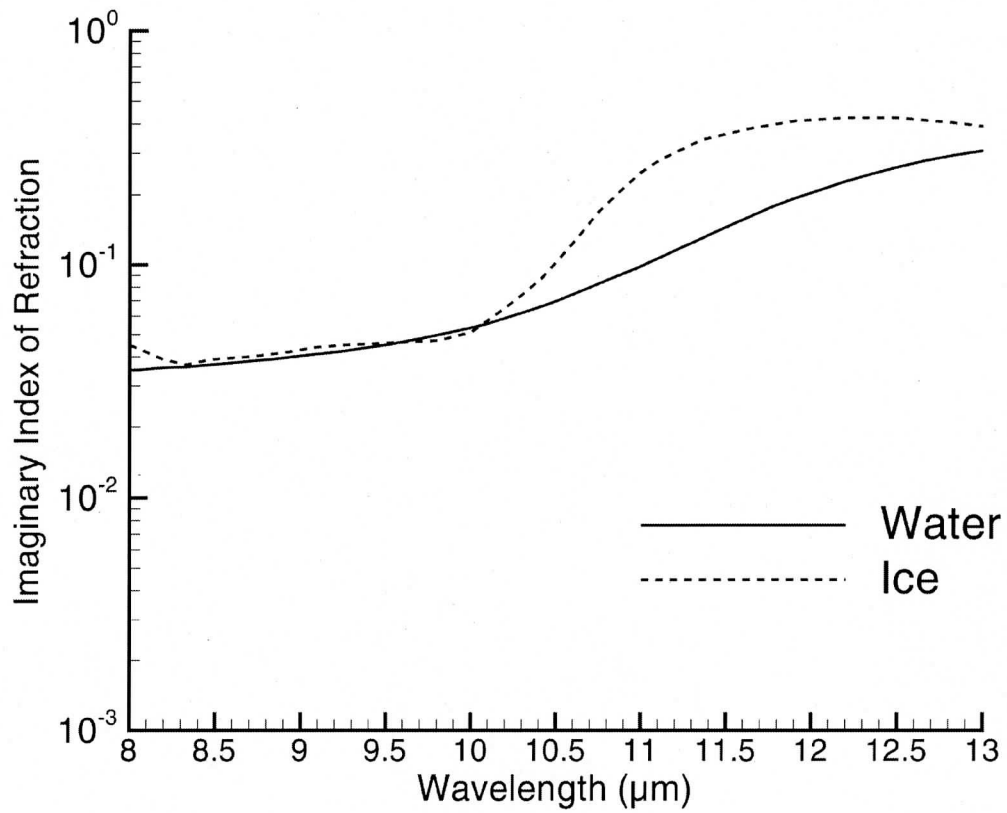


Figure 1: Imaginary index of refraction for water and ice between 8 and 13  $\mu\text{m}$ .

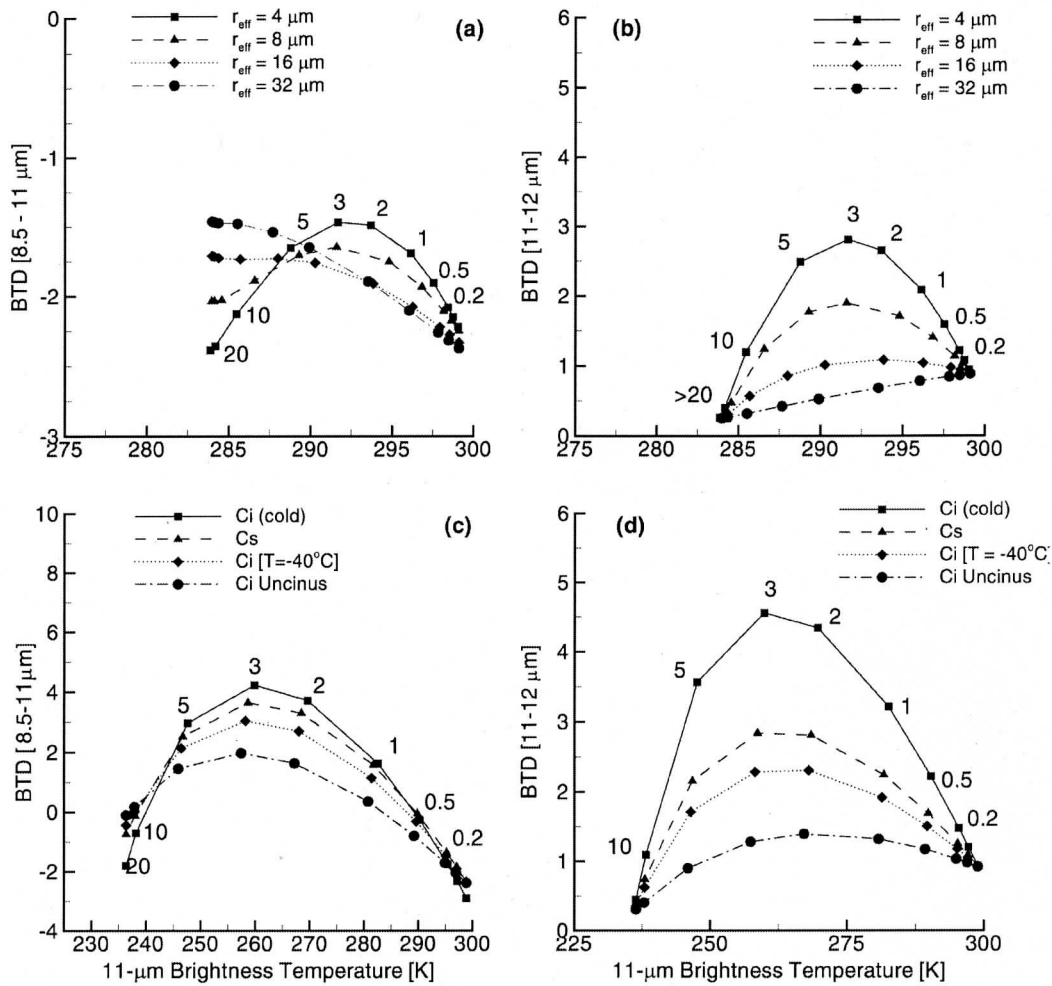
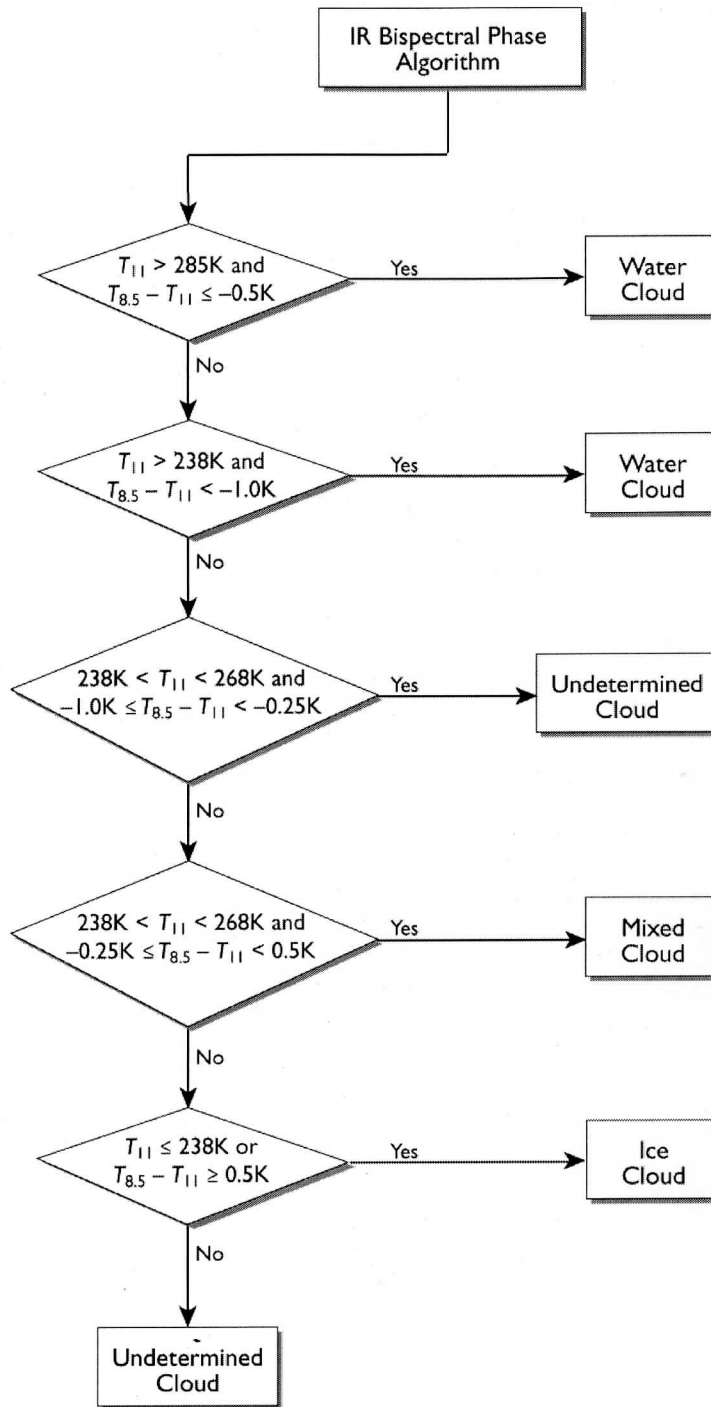
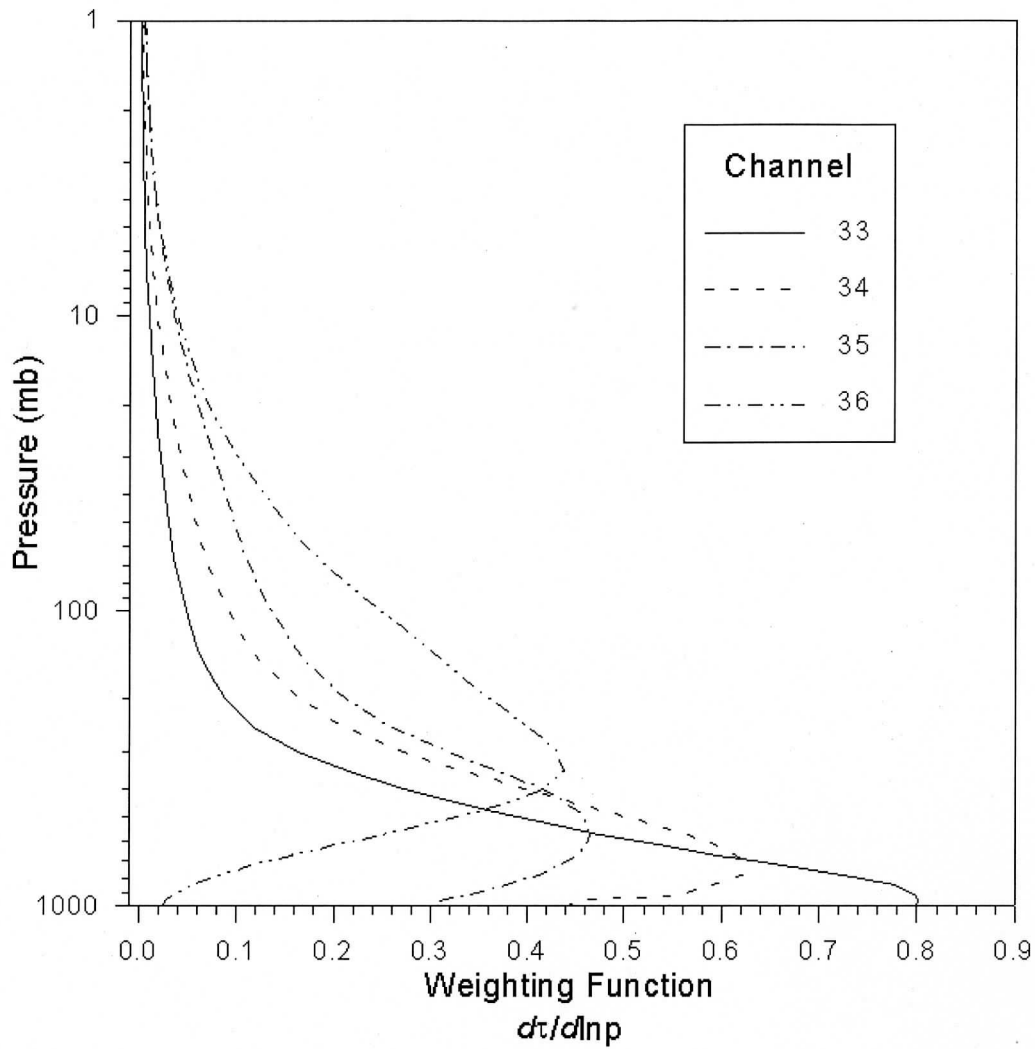


Figure 2: RT calculations for a. BTD[8.5-11] for water cloud, b. BTD[11-12] for water cloud, c. BTD[8.5-11] for ice cloud, d. BTD[11-12] for ice cloud.





**Figure 3: Decision tree for MODIS IR cloud phase determination. Note that the current methodology has static thresholds that are not dependent on the viewing (or scan) angle or surface ecosystem.**



**Figure 4. Weighting functions for the four MODIS channels in the CO<sub>2</sub> absorption band**

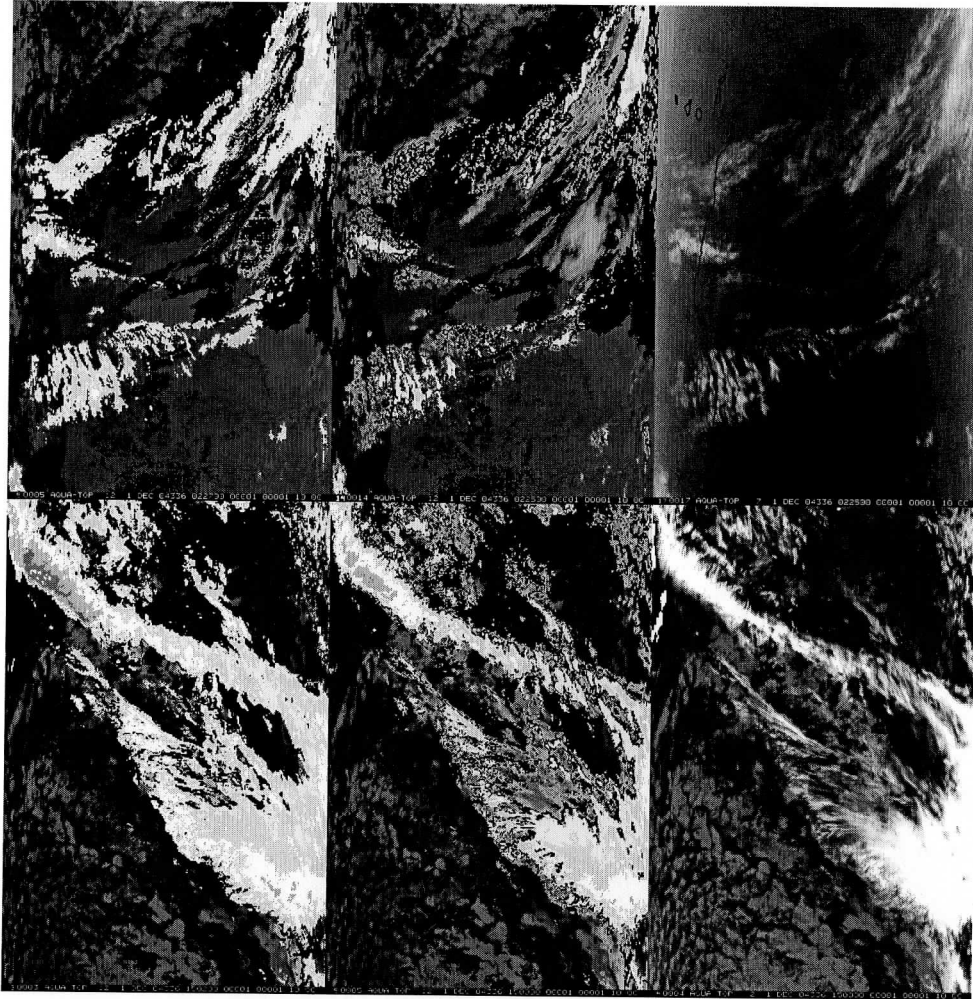


**Figure 5: MODIS Aqua CTP results (CTP < 400 in color) for two different scenes on 1 December 2004 after radiance bias adjustment (left panel), before radiance bias adjustment (middle panel), and black and white infrared image of the scene (right panel). White indicates clouds between 95 and 125 hPa, red 125 and 160 hPa, orange 160 and 190 hPa, yellow 190 and 225 hPa, aqua 225 and 260 hPa, cyan 260 and 300 hPa, sky 300 and 330 hPa, blue 330 and 360 hPa, and navy 360 and 390 hPa.**

## MODIS Cloud Top Height Validation

Comparisons to ER-2 based CPL Lidar, Dec 11, 2002 (1910 - 1920 UTC)

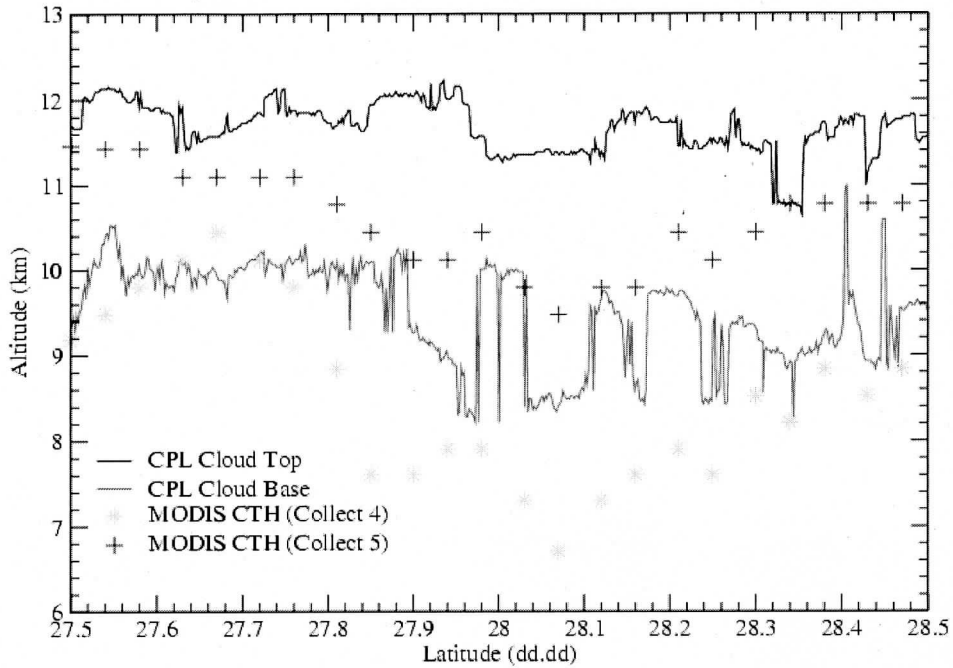


**Figure 6. Comparison of Cloud Physics Lidar determinations of cloud top and bottom with the Collect 5 MODIS cloud top heights (inferred from pressure using the Global Forecast System pressure profiles) over cirrus clouds on 11 December 2002.**

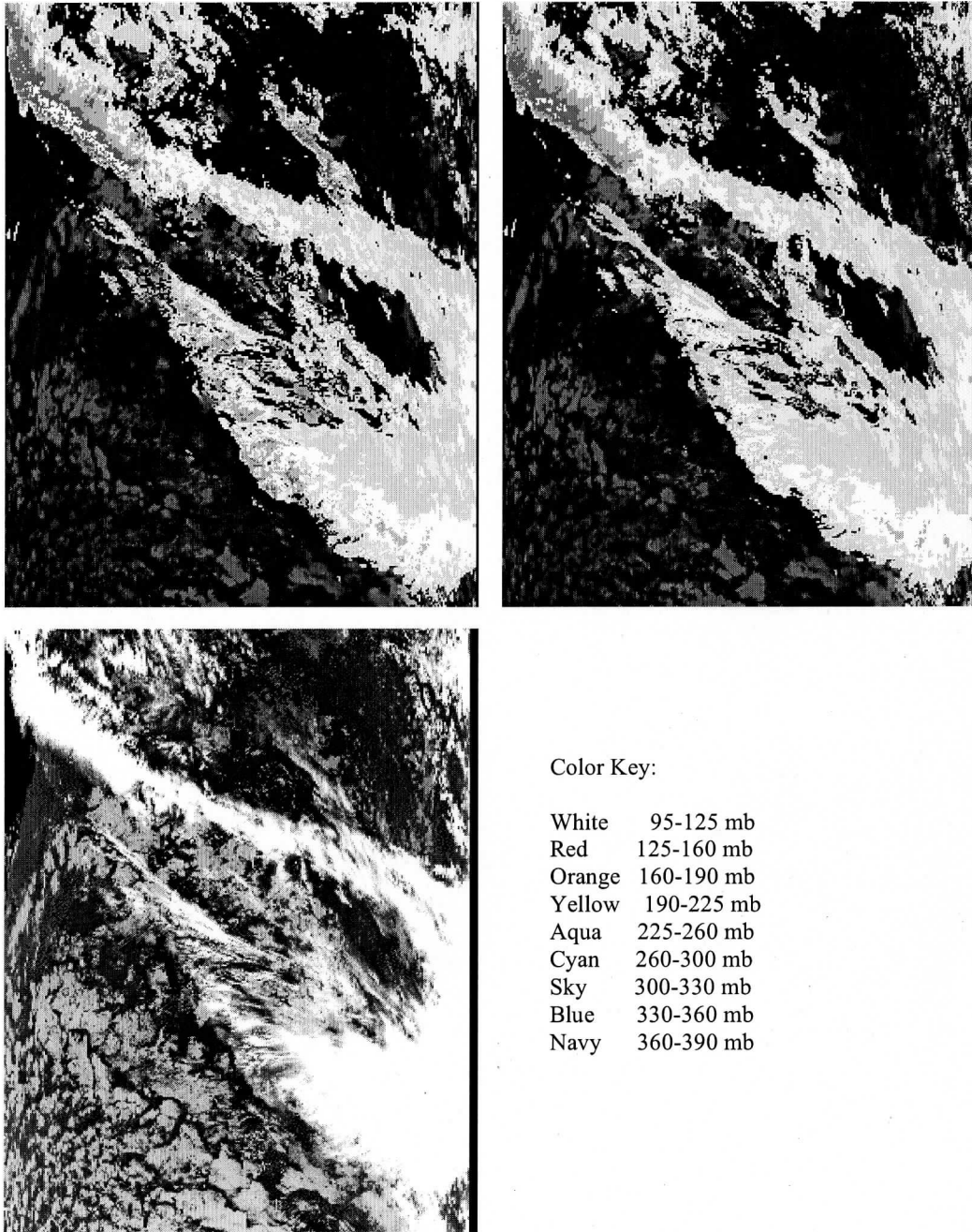


**Figure 7. MODIS granule from 1 December 2004 located in the subtropical N. Atlantic. Top left shows cloud top pressures using original method of choosing final cloud top pressure solution (error minimization technique), top right shows new results using “top-down” method. Only high clouds are shown in colors. Bottom left shows band 31 (11.1  $\mu\text{m}$ ) brightness temperature image.**

25 OCT 90

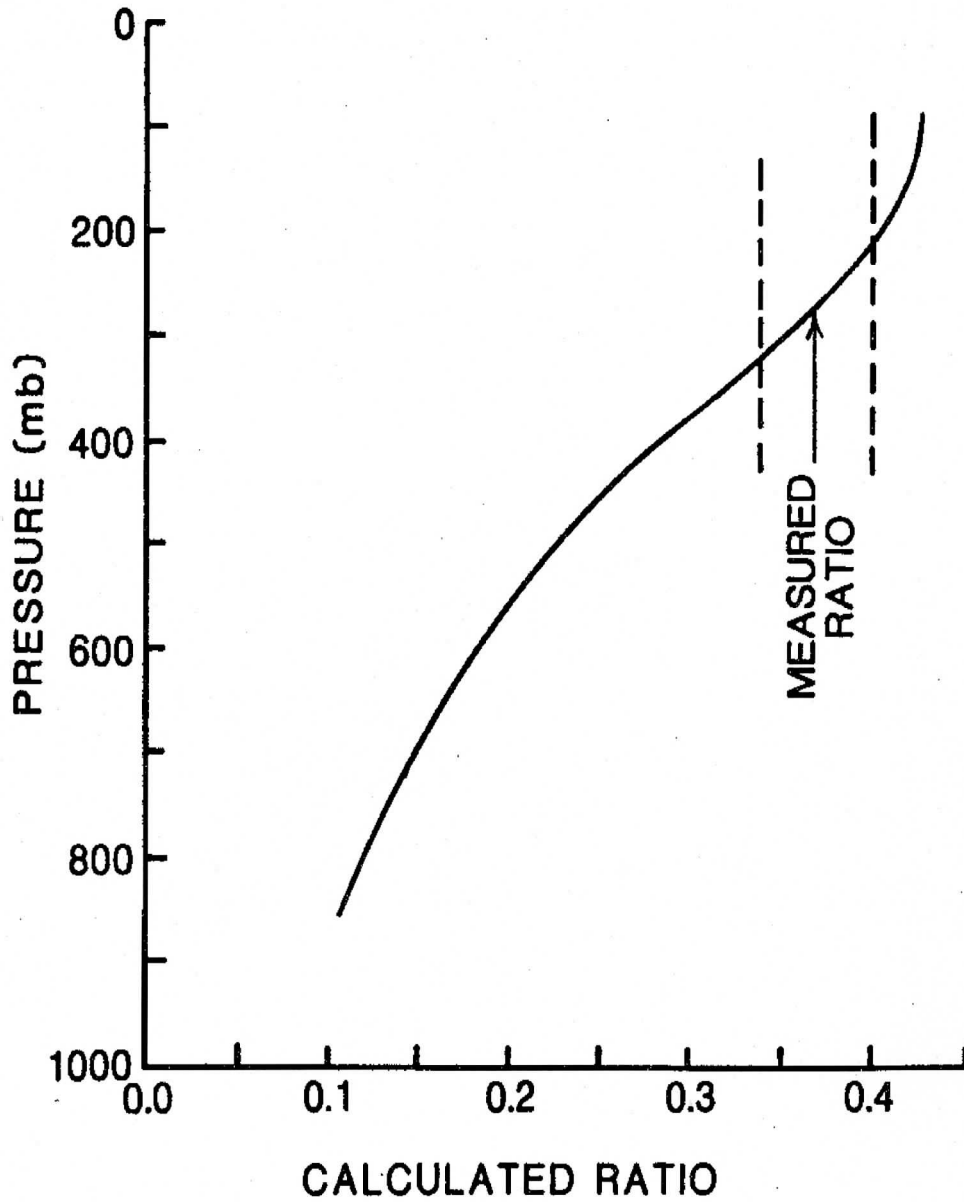


Figure 8. The calculated ratio from the right side of Equation 3 as a function of cloud top pressure from the sounding of 25 October 1990. The measured ratio from the left side of Equation 3 is indicated. The cloud top pressure is inferred to be 300 mb.

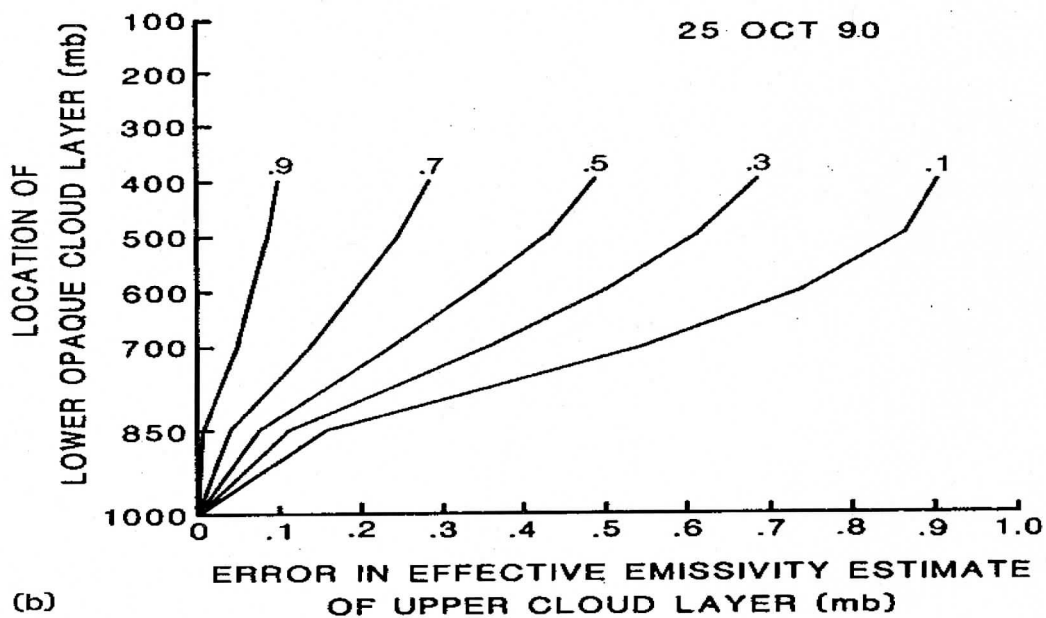
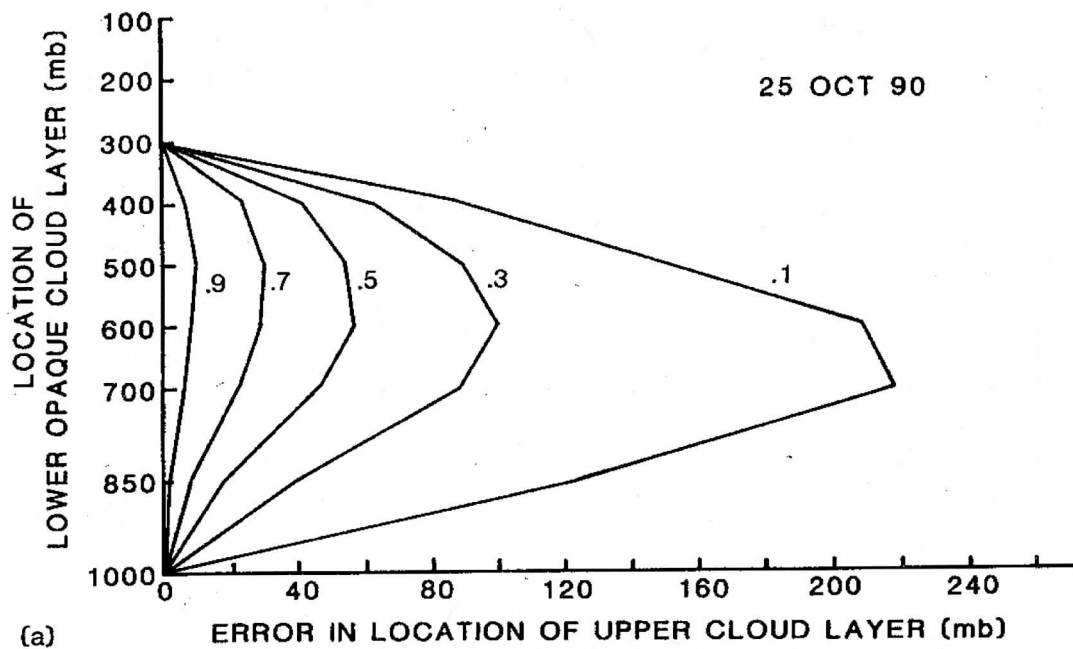
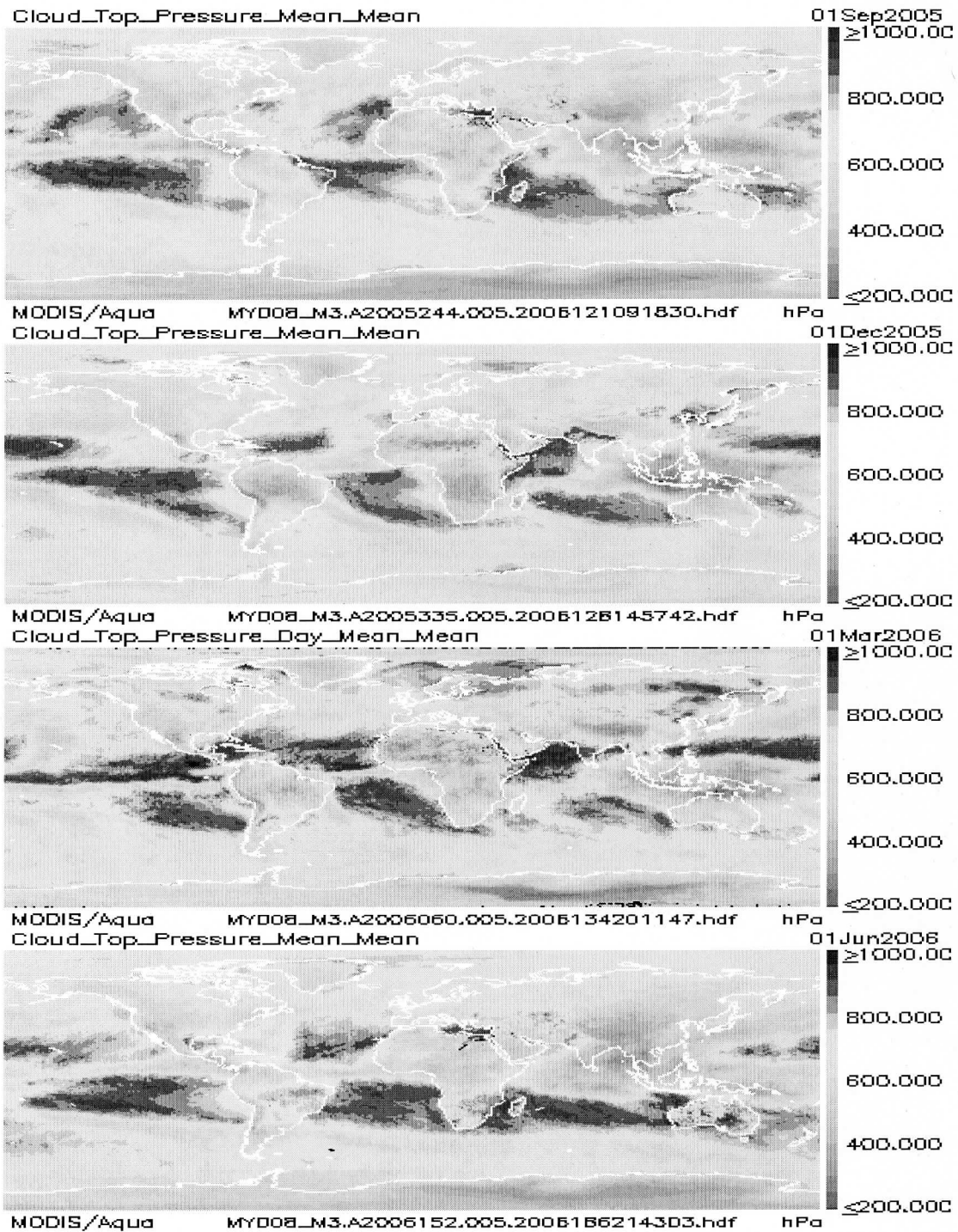


Figure 9. (a) The errors in calculated cloud top pressure (from the original 300 mb solution) for several different NE as a function of height of the underlying opaque cloud layer. (b) The associated errors in effective emissivity (from the original solution of NE).



**Figure 10: 8-day global distributions of MODIS / Aqua mean cloud top pressures (in hPa compiled for 1 x 1 degree gridded latitude-longitude boxes from the previous eight days) on 1 September 2005, 1 December 2005, 1 March 2006, and 1 June 2006 found at <http://modis-atmos.gsfc.nasa.gov/>. Red indicates clear sky.**